Natural loss of function of ephrin-B3 shapes spinal flight circuitry in birds

Baruch Haimson[1], Oren Meir[1], Reut Sudakevitz-Merzbach[1], Gerard Elberg[1], Samantha Friedrich[3], Peter V. Lovell[3], Sónia Paixão[2], Rüdiger Klein[2], Claudio V. Mello[3*] and Avihu Klar[1*]

1 - Department of Medical Neurobiology, IMRIC, Hebrew University-Hadassah Medical School, Jerusalem, 91120, Israel

2 - Department 'Molecules – Signals – Development, Max Planck Institute of Neurobiology, Am Klopferspitz 18, 82152 Martinsried, Germany

3- Department of Behavioral Neuroscience, Oregon Health and Science University, Portland, Oregon, USA.

* - Corresponding authors

Avihu Klar
Department of medical Neurobiology
Hadassah Medical School
The Hebrew University, Jerusalem
91120
Israel
avihu.klar@mail.huji.ac.il

Claudio V. Mello
Department of Behavioral Neuroscience
Oregon Health and Science University
Portland, Oregon
USA
melloc@ohsu.edu

Abstract

Flight in birds evolved through patterning of the wings from forelimbs and transition from alternating gait to synchronous flapping. In mammals, the spinal midline guidance molecule ephrin-B3 instructs the wiring that enables limb alternation, and its deletion leads to synchronous hopping gait. Here we show that the ephrin-B3 protein in birds lacks several motifs present in other vertebrates, diminishing its affinity for the EphA4 receptor. The avian *ephrin-B3* gene lacks an enhancer that drives midline expression, and is missing in Galliformes. The morphology and wiring at brachial levels of the chick spinal cord resemble those of *ephrin-B3* null mice. Importantly, dorsal midline decussation, evident in the mutant mouse, is apparent at the chick brachial level, and is prevented by expression of exogenous *ephrin-B3* at the roof plate. Our findings support a role for loss of ephrin-B3 function in shaping the avian brachial spinal cord circuitry and facilitating synchronous wing flapping.

Teaser:

Walking vs flying: Deciphering the organization and evolution of the neuronal network that controls wing flapping in birds.

46 **Introduction**

47 A critical aspect of locomotion is left-right coordination. Limb alternation is the predominant gait
48 mode in some amphibians (salamanders), reptiles and terrestrial mammals, while synchronous
49 movements are manifested in the legs of other amphibians (frogs) and some marsupials, and in
50 the wings of bats and birds. Based on classical electrophysiological studies in cats and rodents, and
51 genetic manipulations of cell fate and axonal trajectories in mice, a modified "half-center
52 oscillator" model has been proposed that explains limb alternations in mammals (*1, 2*). The core
53 elements are mutually inhibitory neuronal centers on each side of the spinal cord that produce
54 oscillatory excitatory output. This output is simultaneously transmitted to interneurons that
55 innervate motoneurons, termed pre-motoneurons (pre-MNs). These include ipsilateral excitatory
56 pre-MNs that activate motor activity on one side, and commissural inhibitory pre-MNs that inhibit
57 motor output on the other side (Fig. 1A) (*3-6*).

58 The axon guidance molecule ephrin-B3 and its cognate receptor EphA4 are key regulators of
59 alternating gait. In this family, ligand binding to the receptor typically results in axonal repulsion
60 (forward signaling), but ephrin receptors can also act as ligands for ephrins (reverse signaling),
61 prompting repulsion or adhesion (*7*). In wt mice, ephrin-B3 serves as a midline repulsive cue,
62 preventing EphA4-expressing axons of excitatory pre-MNs from aberrantly crossing the ventral
63 and dorsal midlines (Fig. 1A) (*8-12*). Transition from left-right alternation to synchrony occurs in
64 mice mutated in the genes encoding ephrin-B3, EphA4, or the downstream signaling molecule α2-
65 chimaerin, referred to as *hop* mutants. These mice show ectopic commissural projections of
66 otherwise ipsilaterally-projecting excitatory pre-MNs (Fig. 1B) and walk with synchronous
67 movements of the hind- and forelimbs, producing a hopping gait. Furthermore, impairment of the
68 neuroepithelial organization of the roof plate (RP), which leads to partial absence of ephrin-B3
69 expression, results in rabbit-like hopping (*13, 14*).

70 Birds have evolved from dinosaurs that use alternating gait (*15, 16*). Their adaptation for
71 flight includes substantial structural specializations of the forelimb and of the spinal cord circuits
72 that enable synchronous limb movements. Classical transplantation experiments in chick support
73 a role for neuronal networks at the lumbar and brachial spinal levels in the control of the
74 locomotion pattern of the hind- and forelimbs, respectively. In chicks where brachial segments are
75 surgically replaced by lumbosacral segments, the movement of the wings become alternation,
76 whereas coordinated flapping movements are not observed (*17*). In the complementary
77 experiment, transplantation of brachial segments to the lumbar cord result in synchronous,
78 hopping-like leg movements (*18*). These findings support the hypothesis that local circuits in the
79 lumbar and brachial spinal cord instruct level-specific alternate or synchronous movements,
80 respectively.

81 Flight requires spinal circuits that enable the bilateral coordination of forelimb movements.
82 It thus seems reasonable to hypothesize that the emergence of synchronous wing flapping in birds
83 involved a transition from ipsilateral excitatory/contralateral inhibitory inputs to a pattern of
84 bilateral co-excitatory input to wing motoneurons. Such a transition likely required changes in the
85 pre-motor spinal wiring. Notably, mutations in the midline guidance molecules Netrin1 or ephrin-
86 B3 in mice lead, respectively, to a reduction in cross inhibition and an increase in cross excitation
87 (*9, 19, 20*). Netrins were initially described in chick, and have well characterized activity and roles
88 in commissural axonal guidance (*21, 22*). However, little is known about ephrin-B3 in chick, and
89 more generally in birds.

90 To explore a possible role of ephrin-B3 in locomotion patterns in birds, we have conducted a
91 set of genomic, molecular and neuroanatomical studies, using both chick and zebra finch as
92 experimental organisms. We found an ephrin-B3 gene ortholog (EFNB3) in several bird species and
93 lineages, however their open reading frames (ORFs) were considerably shorter, and some domains

critical for forward and reverse signaling were absent or heavily modified compared to non-avian tetrapods. We also observed marked loss of dorsal midline ephrin-B3 expression in the brachial spinal cord of zebra finch, likely due to an avian loss of a critical enhancer element. An EFNB3 ortholog could not be found in chicken and related species, suggesting a gene loss in Galliformes. Spinal cord interneurons in chick showed extensive dorsal midline crossing at brachial levels, similar to ephrin-B3 null mice. In contrast, we observed little dorsal crossing at lumbar levels due to the presence of the glycogen body, which serves as a physical barrier to neurite crossing. The crossing at brachial levels was largely prevented by dorsal midline expression of mouse ephrin-B3. These findings are consistent with a role of ephrin-related mechanisms in spinal wiring patterns that may subserve limb alternation. They also support the notion that diminished barriers to dorsal midline crossing may have favored synchronous limb movements and facilitated the origin and/or maintenance of coordinated flight in birds.

107 **Results**

108 EFNB3 gene in birds

109 We have conducted an extensive and thorough analysis of the genomic region containing
110 EFNB3 and syntenic genes in birds and non-avian outgroups. Our approach required extensive
111 curation of gene predictions in annotated databases, permissive BLAST searches of genomes, WGS
112 databases and p-reads (from Pacbio assemblies) using avian EFNB3 and syntenic gene queries, and
113 RefSeq alignment searches of unplaced genomic scaffolds and reads (details in Methods). We
114 found EFNB3 in a broad range of bird species and orders, including several songbirds, some eagles,
115 an owl, a few cormorants, as well as the seriema, a hummingbird, a ruff, a crane, a stork, and
116 some Anseriformes (duck and goose). WRAP53 was immediately upstream of EFNB3 in all birds
117 where synteny could be examined and in all non-avian organisms studied, including mammals,
118 non-avian sauropsids and amphibians (examples in Fig. 1C,D), providing strong support for EFNB3
119 orthology. A gene prediction was present in only few species, whereas in several others EFNB3
120 was partial, possibly due to incomplete sequences in Illumina assemblies.

121 Notably, we could not identify EFNB3 in any Galliformes (Fig. 1D, red square), even in
122 species with high quality Pacbio assemblies and no local gaps. In chicken, the genes immediately
123 syntenic to EFNB3 in other birds (WRAP53 and KDM6B) were on different chromosomes,
124 suggestive of a local inter-chromosomal rearrangement in this species, with no trace of EFNB3
125 (Fig. 1D, chicken). EFNB3 was also absent in the chicken WGS and Pacbio p-reads, and in numerous
126 RNAseq databases. In quail, a WRAP53 prediction and an unannotated KDM6B (found by BLAST)
127 were found on the same incomplete scaffold. Several Pacbio p-reads from the current assembly
128 (*23*) bridged the local gaps but revealed no trace of EFNB3 (Fig. 1D, quail). EFNB3 was also not
129 detected in the assemblies or WGS of other Galliformes (turkey, pheasant, guinea fowl), even
130 though the syntenic genes were sometimes present in unplaced scaffolds (not shown). A scaffold

131 in the unannotated sage grouse genome contained traces of WRAP53 and KDM6B but no evidence
132 of EFNB3 sequences (Fig. 1D, sage grouse). We also could not find EFNB3 in ratites, but the data
133 were too sparse to conclusively prove or disprove an EFNB3 loss in this basal group
134 Importantly, in most birds where EFNB3 synteny could be verified KDM6B was immediately
135 downstream, whereas in non-avian sauropsids and mammals DNAH2 was interposed between
136 EFNB3 and KDM6B (Fig. 1D, blue). Given there were no gaps in several avian assemblies between
137 EFNB3 and KDM6B, this observation supports an avian-specific loss of DNAH2, as previously
138 indicated (Lovell et al., 2014). As we show later, this finding has important implications for EFNB3
139 expression regulation. The exception among birds was the kakapo, where the receptor gene
140 EphB4 was downstream of EFNB3, the only such case we are aware of. In sum, the EFNB3 gene is
141 clearly present in a broad range of Neoaves, as well as in Anseriformes, but seems absent in
142 Galliformes as a group (Fig. 1C,D). We suggest this is possibly due to a loss that occurred after their
143 split from Anseriformes, an estimated 46 million years ago (*16*), but prior to their later
144 diversification.
145
146 **EFNB3 gene and protein structure in songbirds**
147 Songbirds were the avian group with the most complete information on EFNB3. In zebra finches,
148 EFNB3 is largely conserved compared to non-avian tetrapods, consisting of 5 exons and a large 3'-
149 UTR (Fig. S1A), but predicted avian ephrin-B3 proteins are shorter compared to amphibian,
150 reptilian and mammalian EFNB3 (247-267 vs 332-340 aminoacid residues; Fig. S2). The
151 intracellular domain is shorter in birds, and while the PDZ motif is intact, the entire SH2/3 binding
152 motif, which is required for reverse signaling (*24, 25*), as well as the tyrosine residues that are
153 phosphorylated upon activation of the reverse signaling in other organisms, are missing (Fig. 1E;
154 Fig. S2), suggesting that reverse signaling is impaired. Birds also lack an extracellular heparin

155 binding motif within the region juxtaposed to the transmembrane (TM) domain (*26, 27*), and
156 several residues in the tetramerization interface within the receptor binding domain (RBD),
157 required for normal signaling through the formation of receptor-ligand (Eph–ephrin) complexes
158 (*28*) (Fig. 1E; Fig. S2). The region in the dimerization interface where an L to P (L111P) substitution
159 leads to a hopping mouse phenotype (*29*) is conserved in birds and shows other substitutions
160 (DLDL_108-111_QRDV) compared to mammals (Fig. S2). Unlike ephrin-B3, the predicted avian
161 ephrin-B1 and ephrin-B2 proteins are highly similar to the mammalian proteins in terms of size,
162 sequence and sub-domain partitioning.

163 To test whether these structural differences affect cell trafficking of the avian ephrin-B3,
164 we expressed an amino-myc tagged isoform of the mouse and zebra finch genes in COS-7 cells.
165 Surface staining revealed that both proteins are presented on the cell membrane (Fig. 2A). Next,
166 we used an assay where a chimeric protein composed of the extracellular domain of chicken
167 EphA4 fused to placental alkaline phosphatase is tested for binding to different EFNB3 orthologs
168 expressed in transiently transfected COS-7 cells, noting that chick and the zebra finch EphA4
169 proteins share 98.4% identity. We found that chicken EphA4 binds mouse EFNB3, but not zebra
170 finch EFNB3 (Fig. 2B,C).

171

172 **Expression of ephrin-B3 in zebra finch**

173 The presence of EFNB3 gene in songbirds prompted us to examine its expression pattern in the
174 zebra finch spinal cord. *In situ* hybridization with antisense riboprobes revealed ephrin-B3 mRNA
175 expression in both the floor plate (FP) and roof plate (RP) of the brachial spinal cord in P0 zebra
176 finches, with apparent lower expression in the RP (Fig. 2D). Quantification confirmed that ephrin-
177 B3 expression is higher in the FP and declines along the RP in the ventral-to-dorsal direction (Fig.

178 2D'). This contrasted with mouse at a comparable developmental stage, where expression is
179 similarly high in both the FP and RP (Fig. 2E), with no dorsal decline (Fig. 2E').
180 We reasoned that the modified ephrin-B3 expression seen in zebra finch compared to
181 mouse might relate to changes in regulatory elements. Using UCSC's genome browser, we
182 searched for enhancer hallmarks in mouse EFNB3 and its flanking genes. We found that mouse
183 DNAH2, located immediately downstream of EFNB3 (Fig. 1D, blue), contains several features
184 consistent with presence of an enhancer element in its 1st intron (Fig. S3). Because the DNAH2
185 gene is not present in birds (Fig. 1D blue; Lovell et al., 2014), birds may lack an important EFNB3
186 enhancer element. To test whether this DNAH2-embedded region would be sufficient to confer
187 midline RP expression in the spinal cord of a bird species, a reporter gene cloned downstream of
188 the putative enhancer element was electroporated into the chick spinal cord at E3. Expression of
189 the reporter in both the FP and RP was evident at E9 and E15 (Fig. 2F,G), similar to mouse where
190 endogenous ephrin-B3 midline expression occurs during embryogenesis and early post gestation
191 (E15 chick is equivalent to mouse P2), and contrasting with the more ubiquitous expression of the
192 co-electroporated GFP under a ubiquitous promoter (Fig. 2F,G, insets). Notably, *DNAH2* is missing
193 in all bird species examined to date but it is present in reptiles (Fig. 1D; (*30*)), suggesting the loss of
194 the EFNB3 regulatory element is specific to the avian lineage.
195
196 **Expression of ephrin-B family ligands and EphA4 in chick spinal cord**
197 We next used *in situ* hybridization to examine expression of ephrin-B1 and -B2 at the chick
198 brachial cord, as both can mediate axonal repulsion through the EphA4 receptor and could thus
199 potentially compensate for an EFNB3 loss. Both ephrin-B1 and B2 were expressed in the FP and RP
200 at E10 (Fig. 3A,C). At E16, when the spinal circuitry elicits simultaneous wing flapping (*31*), ephrin-
201 B1 expression persisted in the FP but dorsally it became restricted to the ventral aspect of the RP

202 (Fig. 3B), whereas ephrin-B2 expression was detected only at the ventral tip of the RP (Fig. 3D).
203 Expression of ephrin-B genes in chick spinal cord is thus largely restricted to the FP, low in ventral
204 RP, and absent in the dorsal RP.

205 Next, we studied the expression of the receptor EphA4. In mouse, interneurons that
206 express EphA4 are excluded from the dorsal midline, but many of these cells invade the dorsal
207 midline in *EphA4* and *ephrin-B3* null mutants (*32*). In the chick, expression is detected throughout
208 the spinal cord gray matter at E10, with high levels in scattered interneurons, in the lateral
209 subdivision of the lateral motor column (LMC_l), and in the medial motor column (MMC), but
210 absent in the dorsal midline (Fig. 3E). At E16, EphA4 shows high expression in discrete cells
211 distributed all over the gray matter, including adjacent to and within the dorsal midline (Fig. 3F,
212 white arrow in inset).

213 When we assigned x-y coordinates to EphA4-expressing cells, we observed their midline
214 invasion at E16 compared to E10 (Fig. 3E',F',G). Thus, the presence of EphA4-expressing neurons in
215 the dorsal midline correlates with the temporal reduction of ephrin-B1-2 levels. Taken together
216 with the lack of ephrin-B3, we conclude that a molecular barrier that prevents midline crossing is
217 missing in the chick dorsal spinal cord. This contrasts markedly with mouse, where midline
218 expression of ephrin-B3 persists at high levels both ventrally and dorsally at post gestation stages
219 (*9*).

220

221 **Extended roof plate of the chick brachial cord**

222 To further investigate how the natural loss of EFNB3 might have affected the organization of the
223 avian spinal cord, we examined several parameters that differ significantly between wt and *hop*
224 mutants, namely the size and axonal decussation at the RP, and the somata distribution and
225 neurotransmitter phenotype of commissural pre-MNs (Figs. 4-6).

226 In wt mice, the length of the FP was relatively constant along the longitudinal axis, but the
227 RP was substantially shorter at limb levels, resulting in low RP:FP ratios at those levels (Fig. S4).
228 Thus, the RP:FP ratio can serve as a reasonable proxy for the size of the RP. The length of the RP at
229 limb levels was markedly enlarged in EphA4 knockout mice (Fig. 4B,D) in comparison to control
230 mice (Fig. 4A,C), with a significantly higher RP:FP ratio in the homozygous mutant (1.68±0.22,
231 mean of RP:FP ratios ± SD) than in control mice (0.34±0.13). In birds, an elongated RP was evident
232 at brachial levels in E15 chick (Fig. 4E) and P8 zebra finch (not shown), with RP:FP ratios of
233 2.18±0.2 and 1.53±0.08, respectively, thus comparable to EphA4 knockout mice (Fig. 4G). Hence,
234 the morphology of the avian brachial RP is similar to that of *hop* mutants. At the lumbar sciatic
235 level, the dorsal midline in birds is occupied by an ovoid gelatinous mass - the glycogen body, an
236 avian specific organ (GB; Fig. 4F) (*33-35*). These features differ from those in alternating limbed
237 reptiles (lizard, turtle) where the RP is short, as in wt mice (*36-38*)
238
239 **Patterns of axonal midline crossing in the chick spinal cord**
240 Axon fibers that cross the RP in rodents originate mostly from sensory neurons and inhibitory
241 interneurons (*39, 40*). To further study the extent of dorsal midline crossing in the chick embryonic
242 spinal cord, we examined immunoreactivity for neurofilament (3A10) and for sensory axons
243 (TAG1) at E15 and E17. We observed neurofilament-positive axons crossing the brachial FP in a
244 tight bundle (Fig. 5A, yellow arrows in insets), whereas those crossing the dorsal midline were less
245 fasciculated and sparsely distributed along the dorsal RP (Fig. 5A, white arrows in insets).
246 Quantification showed that 44.8±23% of midline crossing axons at the brachial level were in the
247 RP (Fig. 5G, brachial). TAG1-expressing sensory axons did not appear to cross the midline at this
248 level (Fig. 5B). To further interrogate midline axonal crossing, a membrane-tethered GFP was
249 electroporated at E3 into one side of the spinal cord. At E15, GFP-labeled axons crossing the

250 ventral and dorsal midline were evident (Fig. 5C, yellow and white arrows in insets). Interestingly,
251 a few labeled cells were apparent on the contralateral side dorsally, suggesting that some cells
252 may migrate through the RP at the brachial level (Fig. 5C, white arrowheads in insets).
253 At the lumbar sciatic level, axonal decussation was apparent only through the FP (Fig. 5D-
254 E), with no axons crossing the GB. At the lumbar crural level, which is devoid of GB, dorsal midline
255 crossing was apparent, with 31±12% of crossing fibers occurring through the RP (Fig. 5F,G, crural).
256 Notably, the sciatic nerve innervates muscles of the shank and foot, while nerves originating from
257 the crural plexus innervate the thigh muscles (*41, 42*). Importantly, in the swing phase of birds, the
258 ankle flexion leads to the elevation of the feet, while the knee is relatively stable. Hence, the
259 sciatic nerve mediates the flexion and extension of the ankle and foot joints during stepping.
260 Significant dorsal midline decussation was also apparent at the cervical, brachial and thoracic
261 levels (Fig. 5G), as well as sacral levels (not shown), suggesting that the GB serves as a physical
262 barrier for axonal decussation at the sciatic plexus level, thus allowing hindlimb alternation. In
263 contrast, dorsal midline crossing at brachial levels correlates with synchronous wing (forelimb)
264 movements, similar to that seen in *hop* mice.
265
266 **Connectivity of pre-MNs in the chick spinal cord**
267 The synchronous gait of *hop* mice results from ectopic midline crossing of excitatory pre-MN
268 through the FP and RP (Fig. 1B) (*9, 43*). To analyze the patterns of connectivity of pre-MNs at the
269 lumbar and brachial levels of the chick, we injected the trans-synaptic PRV virus (*44, 45*) into the
270 leg, the distal wing musculature, and the main flight muscle, the pectoralis major. We observed
271 substantial differences in the densities and laminar distributions of commissural pre-MNs (cpre-
272 MNs) at lumbar versus brachial levels (Fig. 6A-C, right side). cpre-MNs accounted for 7.81% of

273 labeled cells at the sciatic level, and for 25.3% and 34.8% of brachial level cells labeled from the
274 distal wing and the pectoral muscle, respectively.

275 The distribution of ipsilateral pre-MNs (ipre-MNs) was similar at lumbar and brachial levels,
276 occupying the medial spinal cord (Fig. 6A-C, left side; Fig. S6). In contrast, the distribution of cpre-
277 MNs was markedly different across levels. At lumbar levels (both sciatic and crural) we observed
278 cpre-MNs ventro-medially, with most cells ventral to the central canal (Fig. 6A, right side; Fig. S6).
279 At the brachial level, cpre-MNs of the distal wing musculature and the pectoral muscle were
280 distributed ventrally and dorsally to the central canal (Fig. 6B-C, right side). Likewise, decussation
281 of pre-MNs differed markedly between lumbar and brachial levels, with axons crossing only the FP
282 at the lumbar level (Fig. 6A'), but both the RP and the FP at the brachial level (Fig. 6B'-C').

283 Synchronous gait in mice *hop* mutants is also associated with pre-MNs that innervate
284 motoneurons bilaterally (*43*). To directly test whether the chick brachial cord contains such cells,
285 we injected PRV-GFP and PRV-cherry into the left and right pectoral muscles, respectively (Fig. 6D,
286 left). 10.9% of pectoral cpre-MNs were double-labelled, most located above the central canal and
287 adjacent to the dorsal midline (Fig. 6D), with neurite processes oriented toward the dorsal midline
288 (Fig. 6D'). Hence, like in *hop* mice, a subpopulation of the brachial pre-MNs innervate
289 motoneurons bilaterally.

290 To examine the neurotransmitter phenotype of spinal pre-MNs, we processed sections
291 from hindlimb and wing PRV-injected embryos for *in situ* hybridization with a marker for excitatory
292 neurons (vGlut2). At the lumbar level, 46.5% of the ipre-MNs and 38.6% of the cpre-MNs were
293 excitatory. At the brachial level, 35% of the ipre-MNs and 38% of the ventral cpre-MNs were
294 excitatory. Of the brachial-specific cpre-MNs that reside dorsal the central canal, 47% were
295 excitatory (Table S1). The chick brachial-specific pre-MNs are thus comparable to the ectopic cpre-
296 MNs in *hop* mutants in location, wiring and excitatory phenotype (*14, 43*).

297

298 **Exogenous ephrin-B3 expression in the chick RP prevents midline axonal crossing**

299 Our observations so far suggest that dorsal midline crossing and the wiring pattern of brachial pre-
300 MNs in chick spinal cord might be linked to a lack of ephrin-B3 expression due to the genomic loss.
301 To test this hypothesis, we examined whether expression of mouse ephrin-B3 in the chick would
302 affect RP neurite crossing. Mouse ephrin-B3 or GFP, cloned into a Cre-dependent expression
303 vector under the RP-specific Wnt1 enhancer element (*46*), were co-electroporated into the E3
304 chick spinal cord (Fig. 7A), and the extent of RP neurite crossing analyzed at E15. To exclude
305 possible effects of exogenous ephrin-B3 in reverse signaling, we also used an ephrin-B3 isoform
306 that lacks the intracellular domain (ephrin-B3-ΔC). Ephrin-B3 expression was confined to the RP
307 (Fig. 7B), and the number of midline crossing neurites was significantly lower for ephrin-B3 (7.1 ±
308 3.1) or ephrin-B3-ΔC (7.1 ± 2.6) than for GFP (16.5 ± 4.6) (Fig. 7C-E). Hence, as in mammals,
309 midline ephrin-B3 expression is sufficient to prevent midline crossing.

310 Next, after targeting ephrin-B3 expression to the RP at E3, PRV was injected into the wing
311 musculature at E14 (Fig. 8A), and the numbers and distribution of cpre-MNs examined at E15.5. In
312 controls, both ipre-MNs and cpre-MNs were seen, the latter both dorsal and ventral to the central
313 canal (Fig. 8B), and their neurites crossed at both the FP and RP (Fig. 8B'). In ephrin-B3-expressing
314 embryos, fewer cpre-MNs were seen, most ventral to the central canal (Fig. 8C,C',C''), and most
315 neurites were observed to cross the FP (Fig. 8C,C',C'', right insets). Short cell extensions, possibly
316 dendrites originating from ipre-MNs, did cross the RP (Fig. 8C, C', right insets). We note that *in ovo*
317 electroporation results in mosaics where only a portion of the cells express the transgene. Our
318 efficiencies varied from 5% to 64% (sections with midline expression of ephrin-B3), thus some
319 axons may circumvent ephrin-B3 and cross the midline close to non-EFNB3 expressing RP cells
320 (Supp movie).

321 Next, we analyzed the spatial distribution of cpre-MNs in five embryos with variable
322 efficiencies of wnt1::ephrin-B3 expression (Fig. 8D). A dorsal to ventral shift in the location of cpre-
323 MNs is apparent when comparing the embryos with lower vs higher exogenous ephrin-B3
324 expression in the RP (1-3 vs 4-5 in Fig. 8D), suggesting a reduction in the size of the brachial-
325 specific dorsal population of cpre-MNs. To further quantify this observation, we subdivided cpre-
326 MNs into ventral and dorsal groups, based on location relative to the central canal, and examined
327 their numbers compared to ipre-MNs. The ratios between pre-MNs populating the different zones
328 were calculated and correlated with the efficiencies of ectopic expression of ephrin-B3, using
329 linear regression (Fig. 8E-H). The ratio of ventral cpre-MNs to ipre-MNs was similar in controls and
330 all experimental embryos (Fig. 8E), thus ephrin-B3 RP expression did not affect this population.
331 The ratio of dorsal cpre-MNs to ipre-MNs was reduced in proportion to higher ephrin-B3
332 expression (Fig. 8F), as was their ratio to ventral cpre-MNs (Fig. 8G). The ratio of all cpre-MNs to
333 the ipre-MNs was also negatively correlated with increasing ephrin-B3 expression (Fig. 8H). We
334 conclude that robust ephrin-B3 RP expression results in fewer cpre-MNs that cross through the RP.
335

336 **Discussion**

337 During vertebrate evolution, most terrestrial species adopted alternating limb motion as an
338 effective gait strategy, while adaptation to powered flight in birds emerged via morphological
339 changes that patterned wings from forelimbs, and required transition from alternate gait to
340 synchronous flapping. Our genomic analysis indicates that the gene encoding the midline axonal
341 repellent ephrin-B3 is missing in chicken and other Galliformes. In songbirds, the EFNB3 gene
342 encodes an ephrin-B3 protein that does not bind to the EphA4 receptor, and whose expression in
343 the spinal cord is reduced along the roof plate, probably due to the loss of a downstream
344 enhancer. Morphological and circuit analyses of the chick spinal cord revealed similarities at the
345 brachial level with mutant mice for components of the ephrin-B3/EphA4 pathway, while at the
346 lumbar level it resembled wt mice (Fig. 8I,J). Importantly, dorsal midline expression of exogenous
347 (rodent) ephrin-B3 in the chick brachial spinal cord prevents crossing of cpre-MN axons.
348 Altogether, our findings support the notion that a reduction in ephrin-B3 expression and/or
349 function plays an important role in shaping the wing level circuitry in the avian spinal cord.

350

351 **Loss of ephrin-B3 function in birds**

352 Changes in gene copy number, enhancers, and protein sequence, arguably some of the foremost
353 molecular events in evolution, are thought to have influenced locomotion patterns in vertebrates.
354 For example, a point mutation that leads to a premature stop codon in *DMRT3* enabled Icelandic
355 horses to develop their characteristic Tölt ambling gait (*47*). A modification and subsequent loss of
356 a regulatory element of *GDF6* during the transition to bipedalism in humans is thought to have
357 played a role in foot digit shortening (*48*). Limb loss in snakes has been shown to be a result of
358 mutations in a limb-specific enhancer of Sonic hedgehog (*49*). Loss of function for ephrin-B3 leads
359 to midline crossing in the spinal cord of rodents, resulting in a remarkable hopping gait (*9, 10*).

360 Our findings now indicate that the ephrin-B3 gene has undergone significant modifications in birds
361 compared to non-avian groups, likely impacting flight control circuits in the avian spinal cord.
362 Absence of *DNAH2* is seen in all birds where this genomic region could be assessed,
363 suggesting that the loss of a putative ephrin-B3 enhancer was an early event in avian evolution, or
364 possibly even in dinosaurs. The apparent loss of EFNB3 in chick and other Galliformes was likely a
365 more recent event specific to that basal clade, since EFNB3 is present in Anseriformes and in
366 several Neoaves, including the more recently evolved Passeriformes. It is hard to estimate the
367 timing of mutations in the coding region, since high quality sequence is limited to a few species.
368 Nonetheless, similar protein changes compared to mammals and non-avian saurospids are present
369 in eagles and in songbirds (Fig. S2), which originated ~65 and ~45 million years ago, respectively
370 (*16*). High-quality sequences of this region in the most basal avian clade, Palaeognathae, currently
371 not available, will be critical for better understanding the timing and extent of avian EFNB3
372 changes.
373 In zebra finch, besides a predicted lack of reverse signaling due to loss of specific domains,
374 we provide clear evidence that forward signaling through the EphA4 receptor is impaired. The lack
375 of binding to avian EphA4, for example, is likely related to substitutions in residues 108-111 (in the
376 mouse protein). This region is within the G β-strand which forms a loop with the H β-strand, and is
377 part of the ligand-receptor dimerization interphase (*50*). The D108Q, L109R and L111V
378 substitutions may therefore affect receptor binding by disrupting the formation of the G-H loop.
379 Interestingly, ephrin-B3 is also a known receptor for the Nipah paramyxovirus (*Henipavirus* group)
380 and the G-H loop is critical for infectivity (*51*), as shown by mutations in the H β-strand of ephrin-
381 B3 (*52*), suggesting possible related changes in spinal circuitry and viral susceptibility mechanisms.
382
383 **Phenotype of avian and *hop* mouse spinal cords**

384 Our data show that the brachial spinal cord of the chick, which lacks an EFNB3 gene, shares
385 similarities with mouse *hop* mutants in its morphology, and in the wiring and excitatory/inhibitory
386 balance of cpre-MNs (Fig. 1B, 8J). The significance of the dorsal midline expansion, anatomically
387 the most profound alteration in *hop* mutants, is unclear. While synchronous motoneuron activity
388 is seen in the spinal cord of *hop* mutants using an *in vitro* fictive locomotion assay, severing of the
389 dorsal midline does not restore left-right alternation (*8, 53*), arguing that bilateral coupling is
390 facilitated by ventral midline crossing. However, *in vivo* disruption of the roof plate integrity is
391 sufficient to induce synchronous gait in mice (*13, 14*). It is conceivable that in *hop* mutants,
392 proprioceptive signals from weight-load receptors, which are used only *in vivo*, inhibit the bilateral
393 coupling mediated by the dorsally crossing axons. In support of this hypothesis, removal of EphA4
394 from a subpopulation of dorsal interneurons results in ectopic dorsal midline crossing.
395 Furthermore, the over-ground gait of these mice is normal, while during air-walking and swimming
396 their limbs move in synchrony (*43*). In birds, dorsal midline crossing might be sufficient to instruct
397 the bilateral coupling of the wings motoneurons, since weight load without ground support during
398 flight does not affect the wings.

399 The importance of excitatory neurons for synchronous gait in mouse *hop* mutants is shown
400 by conditional targeting of EphA4 in vGlut2 neurons, which results in hopping gait (*8*).
401 Furthermore, a rather small shift in the excitatory/inhibitory balance in cpre-MNs, from 21%
402 excitatory and 46% inhibitory in wt to 26% and 35% in the EphA4 null mouse, is sufficient to
403 induce synchronous gait (*9, 53*). We found that the brachial dorsal population of cpre-MNs in chick
404 is moderately but significantly more enriched (–47%) with excitatory neurons than in wt mice.
405 Furthermore, the difference between this population and the brachial ventral and lumbar cpre-
406 MNs, 38% and 35% of excitatory neurons, respectively (Fig. 6, Table S1), is similar to the difference
407 between wt and *hop* mutant mouse. These observations support the notion that the brachial-

408 specific population of cpre-MNs is sufficient to support synchronous activation of motoneurons
409 involved in wing flapping.

410 Intriguingly, *t*he glycogen body (GB) (Fig. 8I) is a prominent but poorly understood dorsal
411 lumbar gelatinous structure that arises from roof plate cells (*33, 34*) and is present across birds
412 (*54, 55*). Our study has uncovered evidence that the GB serves as a major physical barrier to dorsal
413 midline crossing at sciatic lumbar levels in the chick. We thus suggest that the GB is likely a major
414 contributor to the alternating gait in birds, analogous to the molecular barriers to midline crossing
415 in mice.

416 In summary, we provide evidence linking loss of ephrin-B3/ EphA4 signaling to the
417 emergence of synchrony-mediating circuitry in the avian brachial spinal cord. While our findings
418 do not exclude the importance of other molecular pathways, they suggest that modulation of
419 ephrin-related mechanisms may have been an important contributor to the origin of flight in birds.
420

421 **Materials and Methods**

422 **Genomics**

423 The EFNB3 genomic region in birds has presented several difficulties for sequencing and
424 assembling, likely due to very high GC content and density of poorly characterized repeat
425 elements. The gene and its syntenic region are not present, or present only in partial form, in most
426 Sanger- and Illumina-based avian assemblies, but are better represented in the more recent
427 PacBio assemblies (Korlach et al., 2017). Furthermore, this region is likely part of a short avian
428 micro-chromosome, which until the recent Swainson's thrush genome had not been assembled
429 and/or annotated in any species. Our current study of EFNB3 in birds has therefore required
430 considerable search, annotation and curation efforts.

431 Briefly, we initially examined the annotated databases (NCBI's RefSeq, Ensembl) available
432 for >50 avian species, searching for gene predictions annotated as EFNB3 or ephrin B3-like, and
433 using reciprocal BLAT alignments and verification of conserved synteny of the predictions to
434 confirm their orthology with humans and non-avian vertebrates. We were able to identify EFNB3
435 and to verify its orthology in seven songbird species (including zebra finch), an eagle, and a parrot
436 (kakapo). Notably, in the Swainson's thrush EFNB3 and syntenic genes have been assigned to
437 chr37, the first case any genes have been assigned to that avian micro-chromosome. We also note
438 that two apparently identical zebra finch EFNB3 models (discontinued Gene IDs: 115492780 and
439 115492629) were present in an unplaced scaffold (NW_022045341.1) of an early PacBio assembly
440 (bTaeGut1_v1.p; (*56*), but have been recently discontinued as this entire region is not present in
441 the latest zebra finch Pacbio assemblies in NCBI. We used the discontinued XM_030261704.1
442 transcript prediction in our study, noting that it is well supported by ESTs and transcriptome data
443 (Fig. S1A,B). Ensembl has EFNB3 predictions for the zebra finch, kakapo, and sparrowhawk, the
444 latter in a short segment and right upstream of KDM6B. We also BLAST searched avian and non-

445 avian RefSeq databases using as queries the genomic regions just downstream of avian gene
446 predictions annotated as WRAP53 (or WD repeat containing antisense to TP53, a.k.a. telomerase
447 Cajal body protein 1), or just upstream of avian gene predictions for KDM6B (or lysine specific
448 demethylase 6B). This effort identified EFNB3 in an owl and in another songbird species, even
449 though no EFNB3 predictions were present. We also BLAST searched all existing avian genomes
450 (May 2020) as well as the respective WGS databases, using as queries the existing avian EFNB3
451 predictions, and manually examined all hits with scores >50, excluding cases that did not show top
452 reciprocal alignments (typically other EFNB family members). This effort identified EFNB3 in a
453 cormorant, and in a few other passerines and Anseriformes with limited synteny information, as
454 well as in several species with incomplete data for synteny verification (a duck, a goose, several
455 other passerines, eagles and cormorants, the seriema, a ruff, a crane, and a stork). As an EFNB3
456 was not present in the current Anna's hummingbird PacBio assembly (the only such case for a
457 non-Galliformes avian PacBio assembly), we also BLAST searched the pre-assembled reads (p-
458 reads) for this assembly, and obtained evidence for an ortholog with similar synteny as in other
459 bird groups. We also conducted BLAST searches for EFNB3 in the current assemblies of chicken
460 (Pacbio-based GRCg6a) and quail (hybrid Coturnix japonica 2.1), as well as in the corresponding
461 Pacbio p-reads and previous assemblies. These searches were extensive and permissive (>30 hit
462 scores), followed by manual verification of detected hits. We also searched the BBSRC ChickEST
463 Database and several brain transcriptome databases at E10, E17, P0 and 10 weeks old chick
464 available in NCBI (ERR2576391, ERR2576392, ERR2576465, ERR2576464, ERR2576488,
465 ERR2576584, ERR2576585, ERS2480079), but found no evidence of EFNB3.
466
467 **Animals**

468 Fertilized White Leghorn chicken eggs (Gil-Guy Farm, Israel) were incubated in standard conditions
469 at 38 °C. All experiments involved with animals were conducted in accordance with the designated
470 Experiments in Animals Ethic Committee policies and under its approval. Experiments were
471 performed on adult male and female mice. EphA4^{lox} mice (*57*) were crossed to PGK-Cre mice (*58*)
472 to generate full knock-out of the EphA4 gene. Animals were kept and used in accordance with
473 regulations from the government of Upper Bavaria.
474
475 **DNA**
476 For the binding assay in COS cells, the mouse ephrin-B3 was cloned into pSecTag-B plasmid (Termo
477 Fisher Scientific, Waltham, USA). Six repeats of the myc epitope were cloned at the carboxyl end
478 of ephrin-B3. For cell surface detection of the mouse ephrin-B3, the kappa chain signal sequence
479 plus 3 repeats of the myc epitope were cloned upstream to amino acid 30 of the mouse gene. The
480 sequence of the full-length zebra finch ephrin-B3 transcript was reconstructed from RNA-seq
481 reads (Fig. S1B,C) using the Trinity platform (*59*). The sequence matched the exonic sequence of
482 the EFNB3 transcript prediction (XM_030261704.1). For cloning the zebra finch ephrin-B3, an
483 optimized sequence (available upon request) of residues 21-171 (Fig. S2), predicted to encode the
484 extracellular domain, was synthesized (ITD, Coralville, USA) and cloned downstream to an Ig kappa
485 chain signal sequence in the pSecTag-B plasmid. The transmembrane and intracellular portions of
486 the zebra finch transcript were obtained by fully sequencing the EST DV945855 cDNA clone. The
487 synthetic 5' portion of the gene plus the 3' DV945855-derived sequence were fused using a PCR-
488 generated EcoRV site at the synthetic 5' part and an internal SmaI site in the 3' DV945855-derived
489 sequence. For detection of the *in vitro* transcribed protein, 4 repeats of the myc epitope were
490 inserted between the Ig kappa chain signal sequence and predicted residue 21 of zebra finch

491 ephrin-B3. The EphA4-AP fused gene was generated by cloning amino acids 1-543 of the chick
492 EphA4 (*60*) into the pSecTag-B plasmid. The SEAP gene was cloned downstream to EphA4.
493
494 **Cell culture and transfection**
495 COS-7 cells (ATCC) were cultured in DMEM media (Sigma, Saint Louis, USA) supplemented with
496 10% fetal bovine serum 100U/ml penicillin, 100 mg/ml streptomycin and 2 mM glutamine
497 (Biological industries, Beit HaEmek, Israel). COS-7 cells were transiently transfected with
498 appropriate cDNA using PEI (Polyethylenimine, linear, MW 25000; Polysciences, Inc).
499
500 **AP-fusion protein binding experiments**
501 To produce secreted EphA4-AP (alkaline phosphatase, placental) fusion protein, COS-7 cells were
502 transiently transfected with appropriate cDNA. Post-transfection cells were supplemented with
503 Opti-MEM (Gibco), and media collected after 48 hr. The media was concentrated through a 30K
504 ultracell filter (Merck Millipore, Tullagreen, Ireland). The amount of the AP fusion protein was
505 quantified by SDS-PAGE analysis and Coomassie staining. The amount of EphA4-AP was calibrated
506 by comparison to known amounts of EphA4-Fc fusion protein (R&D, Indinapolis, USA). AP activity
507 was measured using para-nitrophenylphosphate substrate (pNPP, Sigma).
508 Binding assays were carried in COS-7 cells, transiently transfected with the mouse or zebra
509 finch ephrin-B3. Following over-night (O/N) incubation, cells were incubated with varying amount
510 of EphA4-AP in binding buffer (Hanks buffer saline supplemented with 20 mM Hepes, PH 7.3,
511 0.05% BSA, 5 mM CaCl2, 1 mM MgCl2 and 10 µg/ml heparin sodium salt (Sigma) at room
512 temperature (RT) for 70 min. For visualization of AP staining, cells were plated on glass coverslip
513 coated with poly-lysine (0.005%, Sigma), and following AP-ligand binding as described above, cells
514 were washed with-binding buffer, fixed in 4% paraformaldehyde (PFA) in PBS for 15 min at RT, and

515 then washed with HBS solution (20 mM HEPES pH 7.3, 150 mM NaCl). Endogenous AP activity was
516 inactivated by incubation at 65 °C for 100 min. For color reaction, cells were incubated with
517 NBT/BCIP substrates (Roche, Basel, Switzerland) in AP buffer (100 mM Tris pH 9.5, 100 mM NaCl,
518 5 mM $MgCl_2$), O/N. After washing in HBS and fixation for 15 min in 4% PFA, and an additional
519 washing in HBS, coverslips were mounted under mounting medium (Thermo Scientific, USA).
520 For colorimetric assays, following AP-ligand binding and washing, cells were incubated O/N
521 at 4°C in lysis buffer (10 mM Tris, ph 8.0, with 1% Triton X100). The supernatant was subjected to
522 heat inactivation for 15 min at 65°C. Lysates were transferred to 96-well high protein absorbance
523 plate (Thermo Scientific, Nunc International USA) and the level of AP activity was determined
524 following addition of equal volume of 2 mg/ml pNPP substrate in reaction buffer (200 mM Tris, pH
525 9.5, 10 mM MgCl2, 200 mM NaCl). Plates were incubated at RT for 30 min to 1 hr and optical
526 density was determined at 405 nM using an ELISA plate reader.
527
528 **Ephrin-B3 surface staining**
529 COS-7 cells were transiently transfected with the mouse or zebra finch myc-EphrinB3 expression
530 vectors. 24 hr post-transfection, cells were incubated with mouse anti-myc (9E10) antibody in
531 phosphate buffered saline (PBS), washed with PBS, and subsequently incubated with Rhodamine
532 Red X (RRX) labeled anti-mouse antibody and washed again. Cells were fixed in 4%
533 paraformaldehyde/0.1 M phosphate buffer and mounted before imaging.
534
535 **In-ovo electroporation**
536 A DNA solution of 5 mg/mL was injected into the lumen of the neural tube at HH stage 17– 18
537 (E2.75-E3). Electroporation was performed using 3 × 50 ms pulses at 25–30 V, applied across the
538 embryo using a 0.5 mm tungsten wire and a BTX electroporator (ECM 830). Following

539 electroporation, 150–300 µL of antibiotic solution, containing 100 unit/mL penicillin in Hank's
540 Balanced Salt Solution (Biological Industry, Beit-Haemek) was added on top of the embryos.
541 Embryos were incubated for 3–19 days prior to further treatment or analysis. Roof plate-specific
542 expression was achieved utilizing the Wnt1 or DNAH2 enhancers, coupled with a dorsal electrode
543 positioning.
544
545 **Immunohistochemistry and *in-situ* hybridization**
546 Embryos were fixed overnight at 4°C in 4% paraformaldehyde/0.1 M phosphate buffer, washed
547 twice with phosphate buffered saline (PBS), incubated in 30% sucrose/PBS for 24 h, and
548 embedded in OCT (Scigen, Grandad, USA). Cryostat sections (20 µm) were collected on Superfrost
549 Plus slides and kept at −20°C. For thicker sections, spinal cords were isolated from the fixed
550 embryos and subsequently embedded in warm 5% agar (in PBS), and 100 µm sections (E12–E17)
551 were cut with a Vibratome. Sections were collected in wells (free-floating technique) and
552 processed for immunolabeling. The following primary antibodies were used: rabbit polyclonal anti-
553 GFP 1:1000 (Molecular Probes, Eugene, Oregon, USA), mouse anti-GFP 1:100, goat anti-GFP 1:300
554 (Abcam, Cambridge, UK), rabbit anti-RFP 1:1000 (Acris, Hiddenhausen, Germany), goat anti-ChAT
555 1:300 (Cemicon, Temecula, CA, USA), mouse anti-neurofilament 1:100 (3A10), mouse anti-myc
556 1:10 (9E10), rabbit anti-myc 1:100 (Abcam). The following secondary antibodies were used: Alexa
557 Fluor 488/647-AffiniPure Donkey anti-mouse, -rabbit and -goat (Jackson), and Rhodamin Red-X
558 Donkey anti-mouse and -rabbit (Jackson). Images were taken under a microscope (Eclipse Ni;
559 Nikon) with a digital camera (Zyla sCMOS; Andor) or a confocal microscope (FV1000; Olympus).
560 *In situ* hybridization was performed as described (Avraham et al., 2010). The following probes
561 were employed: chick ephrin-B1, ephrin-B2, EphA4 and Vglut2, zebra finch ephrin-B3 and mouse
562 ephrin-B3. Probes were PCR-amplified from brain cDNAs of E6 chick embryo, P4 zebra finch, and

563 E15 mouse, respectively, using the following primers. PCR products were verified by sequencing

564 prior to use.

Name	Sequence
cEFNB1-F	GAAAAAGGACCAGGCAGATGC
cEFNB1-R-T7	AGCTAATACGACTCACTATAGTTCTCTGTAGTCCGTAAGGG
cEFNB2-F	GAGGGGTGTGCCAGACAAAA
cEFNB2-R-T7	AGCTAATACGACTCACTATAGCACTGTCTGCAGTCCTTAGAG
cEPHA4-F	ACAGGCCCAATGGAGTCATC
cEPHA4-T7	AGCTAATACGACTCACTATAGGCATCCAAGGAGCCATTCTC
mEFNB3-F2	CCAGAACAGGAAGTCGCACT
mEFNB3-T7	AGCTAATACGACTCACTATAGCAAGACAAATTGGGCCTGCC
vGlut2-F	GGAAGATGGGAAGCCCATGG
vGlut2-T7	GAAGTCGGCAATTTGTCCCC
zfEFNB3_3'-F-T3	GCAATTAACCCTCACTAAAGGCACGCCCACAAAGGGAAGGA
zfEFNB3_3'-R-T7	AGCTAATACGACTCACTATAGTCTAATCAGCAGCAGCCGCG
zfEFNB3_5'-F-T3	GCAATTAACCCTCACTAAAGGTTACGTGCTGTACCCGCAGAT
zfEFNB3_5'-R-T7	AGCTAATACGACTCACTATAGCTCGTCTGATTGGCTGAACCT

565

566 **PRV injection**

567 We used two isogenic recombinants of an attenuated PRV strain (PRV Bartha) that express
568 enhanced GFP (PRV152) and monomeric red fluorescent protein (PRV614). The viruses were
569 harvested from Vero cell cultures at titers 4 × 108, 7 × 108 and 1 × 109 plaque forming units
570 (pfu/mL), respectively. Viral stocks were stored at −80°C. For pre-motoneuron infection, injections
571 of 3 µL of PRV152 or PRV614 were made into the thigh or wing musculature of E13 or E14 chick
572 embryos, using Hamilton syringes (Hamilton; Reno, NV, USA) equipped with a 33-gauge needle.
573 The embryos were incubated for 36–40 hr and sacrificed for analysis. For bilateral pre-
574 motoneurons infection, PRV152 and PRV614 were each injected into the pectoralis musculature
575 on opposite sides of the embryo midline.
576

577 **Cell distribution and density plots construction**

578 The codes for the cell distribution and density plots imaging and analysis were written in Matlab.
579 The distribution plots were constructed by calculating the relative midline expression, after
580 background subtraction and a subsequent length normalization between all analyzed sections. The
581 density plots were generated based on cross section images transformed to a standard form. The
582 background was subtracted, and the cells were filtered automatically based on their soma area or
583 using a manual approach. Subsequently, the neurons were depicted by semi-transparent circles or
584 their distribution was visualized by two-dimensional kernel density estimation, using the MATLAB
585 function “kde2d”. Unless indicated otherwise, a contour plot was drawn for density values
586 between 20% and 80% of the estimated density range, in six contour lines. An additional script
587 was used for pre-motoneuron classification based on their neurotransmitter identity and laminar
588 location.
589 A similar density visualization procedure was done for the EphA4 density plots (Fig. 3E’ and F’), but
590 was preceded by signal binarization and then an averaging filter (5 cycles) was used to achieve a

591 smoother density signal. The intensity of EphA4 signal as a function of distance from the midline
592 was obtained by summation of the binary signal over the horizontal axis, followed by a rescaling
593 step for each image. Statistical analysis was done after subdividing the distance around the dorsal
594 midline spanning from -15 to 15 (the relative distance between the central canal – 0, and the
595 white/gray matter boundary – 100 and -100). into 6 equal intervals, and t-test was performed for
596 the grouped data of each interval, originating from E10 and E16 data.

597 **Statistical Analysis**

598 Fig. 3I.
599

Distance from midline	-15 to -10	-10 to -5	-5 to -1	0 to 5	5 to 10	10 to 15
p-value (t-test)	1.3E-24	3.29E-44	4.38E-26	1.07E-98	1.1E-121	4.27E-26

600

Fig. 4G.

Quantiles

Level	Minimum	10%	25%	Median	75%	90%	Maximum
1_Mouse EphA4 Het (n=3)	0.1875	0.2	0.266667	0.296703	0.450321	0.535417	0.75
2_Mouse EphA4 KO(n=3)	1.304348	1.396667	1.508333	1.699095	1.857143	1.979861	2.25
3_Chicken (n=2)	1.76087	1.917544	2.06875	2.132456	2.385346	2.482353	2.578947
4_ZF (n=1)	1.333333	1.405848	1.491071	1.536585	1.604167	1.622017	1.681818

Means and Std Deviations

Level	Number	Mean	Std Dev	Std Err Mean	Lower 95%	Upper 95%
1_Mouse EphA4 Het (n=3)	36	0.3476214	0.1355198	0.0225866	0.3017681	0.3934747
2_Mouse EphA4 KO(n=3)	36	1.6895941	0.2226598	0.03711	1.6142568	1.7649313
3_Chicken (n=2)	22	2.1805534	0.2087605	0.0445079	2.0879941	2.2731126
4_ZF (n=1)	25	1.5334836	0.0831688	0.0166338	1.4991531	1.567814

Means Comparisons

Comparisons with a control using Dunnett's Method

Control Group = 1_Mouse EphA4 Het (n=3)

Confidence Quantile

|d|	Alpha
2.39255	0.05

LSD Threshold Matrix

Level	Abs(Dif)-LSD	p-Value
3_Chicken (n=2)	1.721	<.0001*
2_Mouse EphA4 KO(n=3)	1.244	<.0001*
4_ZF (n=1)	1.078	<.0001*
1_Mouse EphA4 Het (n=3)	-0.1	1.0000

Positive values show pairs of means that are significantly different.

Fig. 5G

Quantiles

Level	Minimum	10%	25%	Median	75%	90%	Maximum
Cervical	0.166667	0.251282	0.5	0.583333	0.75	0.9	1
Brachial	0.076923	0.214907	0.294118	0.384615	0.545455	0.822222	1.2
Thorax	0.304348	0.377778	0.470588	0.555556	0.727273	1	1.166667
Crural	0.125	0.131594	0.1875	0.315789	0.4	0.477778	0.571429
Sciatic	0	0	0	0	0	0	0

Means and Std Deviations

Level	Number	Mean	Std Dev	Std Err Mean	Lower 95%	Upper 95%
Cervical	15	0.6103012	0.2033028	0.0524926	0.4977158	0.7228865
Brachial	31	0.4487473	0.2349142	0.0421918	0.36258	0.5349145
Thorax	27	0.6096124	0.2135042	0.0410889	0.525153	0.6940719
Crural	23	0.311106	0.1260886	0.0262913	0.2565812	0.3656308
Sciatic	14	0	0	0	0	0

Fig. 7E.

Quantiles

Level	Minimum	10%	25%	Median	75%	90%	Maximum
GFP	8	9.9	13.25	16	20	23	29
mEFNB3	2	4	4	7	10	12	13
mEFNB3-S	3	4	5	7	9	11	13
zf-EFNB3	9	9	11	13	16	21	21

Means and Std Deviations

Level	Number	Mean	Std Dev	Std Err Mean	Lower 95%	Upper 95%
GFP	48	16.5208	4.72202	0.68156	15.150	17.892
mEFNB3	42	7.1667	3.21518	0.49611	6.165	8.169
mEFNB3-S	47	7.1277	2.66717	0.38905	6.345	7.911
zf-EFNB3	39	13.9744	3.72394	0.59631	12.767	15.182

Means Comparisons

Comparisons with a control using Dunnett's Method

Control Group =

GFP

LSD Threshold Matrix

Level	Abs(Dif)-LSD	p-Value
GFP	-1.78	1.0000
zf-EFNB3	0.663	0.0045*
mEFNB3	7.509	<.0001*
mEFNB3-S	7.601	<.0001*

Positive values show pairs of means that are significantly different.

645 Fig. 8E-8H
646
647 **R squared values:**
648
649 E. $R^2 = 0.086$
650 F. $R^2 = 0.9066$
651 G. $R^2 = 0.7469$
652 H. $R^2 = 0.7511$

653

654

655 **References**

656 1. T. G. Brown, On the nature of the fundamental activity of the nervous centres; together with
657 an analysis of the conditioning of rhythmic activity in progression, and a theory of the
658 evolution of function in the nervous system. *J Physiol* **48**, 18-46 (1914).
659 2. I. A. Rybak, N. A. Shevtsova, O. Kiehn, Modelling genetic reorganization in the mouse
660 spinal cord affecting left-right coordination during locomotion. *J Physiol* **591**, 5491-5508
661 (2013).
662 3. W. A. Alaynick, T. M. Jessell, S. L. Pfaff, SnapShot: spinal cord development. *Cell* **146**,
663 178-178 e171 (2011).
664 4. M. Goulding, Circuits controlling vertebrate locomotion: moving in a new direction. *Nature*
665 *reviews. Neuroscience* **10**, 507-518 (2009).
666 5. S. Grillner, A. El Manira, Current Principles of Motor Control, with Special Reference to
667 Vertebrate Locomotion. *Physiol Rev* **100**, 271-320 (2020).
668 6. S. Grillner, T. M. Jessell, Measured motion: searching for simplicity in spinal locomotor
669 networks. *Current opinion in neurobiology* **19**, 572-586 (2009).
670 7. A. Kania, R. Klein, Mechanisms of ephrin-Eph signalling in development, physiology and
671 disease. *Nat Rev Mol Cell Biol* **17**, 240-256 (2016).
672 8. L. Borgius *et al.*, Spinal glutamatergic neurons defined by EphA4 signaling are essential
673 components of normal locomotor circuits. *J Neurosci* **34**, 3841-3853 (2014).
674 9. K. Kullander *et al.*, Role of EphA4 and EphrinB3 in local neuronal circuits that control
675 walking. *Science* **299**, 1889-1892 (2003).
676 10. K. Kullander *et al.*, Ephrin-B3 is the midline barrier that prevents corticospinal tract axons
677 from recrossing, allowing for unilateral motor control. *Genes Dev* **15**, 877-888 (2001).
678 11. H. Wegmeyer *et al.*, EphA4-dependent axon guidance is mediated by the RacGAP alpha2-
679 chimaerin. *Neuron* **55**, 756-767 (2007).
680 12. N. Yokoyama *et al.*, Forward signaling mediated by ephrin-B3 prevents contralateral
681 corticospinal axons from recrossing the spinal cord midline. *Neuron* **29**, 85-97 (2001).
682 13. K. Katayama, J. R. Leslie, R. A. Lang, Y. Zheng, Y. Yoshida, Left-right locomotor circuitry
683 depends on RhoA-driven organization of the neuroepithelium in the developing spinal cord.
684 *J Neurosci* **32**, 10396-10407 (2012).
685 14. S. Skarlatou *et al.*, Afadin Signaling at the Spinal Neuroepithelium Regulates Central Canal
686 Formation and Gait Selection. *Cell Rep* **31**, 107741 (2020).
687 15. K. Padian, L. M. Chiappe, The origin of birds and their flight. *Sci Am* **278**, 38-47 (1998).
688 16. R. O. Prum *et al.*, A comprehensive phylogeny of birds (Aves) using targeted next-
689 generation DNA sequencing. *Nature* **526**, 569-573 (2015).
690 17. K. Straznicky, Function of Heterotopic Spinal Cord Segments Investigation in the Chick.
691 *Acta Biol Acad Sci Hung* **14**, 143-153 (1963).
692 18. C. H. Narayanan, V. Hamburger, Motility in chick embryos with substitution of lumbosacral
693 by brachial and brachial by lumbosacral spinal cord segments. *J Exp Zool* **178**, 415-431
694 (1971).
695 19. N. Rabe Bernhardt *et al.*, DCC mediated axon guidance of spinal interneurons is essential
696 for normal locomotor central pattern generator function. *Developmental biology* **366**, 279-
697 289 (2012).
698 20. N. Rabe, H. Gezelius, A. Vallstedt, F. Memic, K. Kullander, Netrin-1-dependent spinal
699 interneuron subtypes are required for the formation of left-right alternating locomotor
700 circuitry. *J Neurosci* **29**, 15642-15649 (2009).
701 21. T. E. Kennedy, T. Serafini, J. R. de la Torre, M. Tessier-Lavigne, Netrins are diffusible
702 chemotropic factors for commissural axons in the embryonic spinal cord. *Cell* **78**, 425-435
703 (1994).

704 22. T. Serafini *et al.*, The netrins define a family of axon outgrowth-promoting
705 proteinshomologous to C. elegans UNC-6. *Cell* **78**, 409-424 (1994).
706 23. K. M. Morris *et al.*, The quail genome: insights into social behaviour, seasonal biology and
707 infectious disease response. *BMC Biol* **18**, 14 (2020).
708 24. C. A. Cowan, M. Henkemeyer, The SH2/SH3 adaptor Grb4 transduces B-ephrin reverse
709 signals. *Nature* **413**, 174-179 (2001).
710 25. Q. Lu, E. E. Sun, R. S. Klein, J. G. Flanagan, Ephrin-B reverse signaling is mediated by a
711 novel PDZ-RGS protein and selectively inhibits G protein-coupled chemoattraction. *Cell*
712 **105**, 69-79 (2001).
713 26. H. L. Holen *et al.*, Ephrin-B3 binds to a sulfated cell-surface receptor. *Biochem J* **433**, 215-
714 223 (2011).
715 27. H. L. Holen *et al.*, Ephrin-B3 binds specifically to B lymphocytes in blood and induces
716 migration. *Scand J Immunol* **74**, 144-154 (2011).
717 28. J. P. Himanen, N. Saha, D. B. Nikolov, Cell-cell signaling via Eph receptors and ephrins.
718 *Curr Opin Cell Biol* **19**, 534-542 (2007).
719 29. C. N. Arnold *et al.*, ENU-induced phenovariance in mice: inferences from 587 mutations.
720 *BMC Res Notes* **5**, 577 (2012).
721 30. P. V. Lovell *et al.*, Conserved syntenic clusters of protein coding genes are missing in birds.
722 *Genome Biol* **15**, 565 (2014).
723 31. V. Hamburger, R. Oppenheim, Prehatching motility and hatching behavior in the chick. *J*
724 *Exp Zool* **166**, 171-203 (1967).
725 32. S. Paixao *et al.*, EphrinB3/EphA4-mediated guidance of ascending and descending spinal
726 tracts. *Neuron* **80**, 1407-1420 (2013).
727 33. L. D. De Gennaro, Origin of the avian glycogen body: I. Effects of tail bud removal in the
728 chick embryo. *Growth Dev Aging* **55**, 19-26 (1991).
729 34. L. D. De Gennaro, Origin of the avian glycogen body. II. Observations in support of a glial
730 nature in the chick embryo. *Growth Dev Aging* **57**, 275-281 (1993).
731 35. R. Necker, The structure and development of avian lumbosacral specializations of the
732 vertebral canal and the spinal cord with special reference to a possible function as a sense
733 organ of equilibrium. *Anat Embryol (Berl)* **210**, 59-74 (2005).
734 36. G. Fabbiani, M. I. Rehermann, C. Aldecosea, O. Trujillo-Cenoz, R. E. Russo, Emergence of
735 Serotonergic Neurons After Spinal Cord Injury in Turtles. *Front Neural Circuits* **12**, 20
736 (2018).
737 37. A. Kusuma, H. J. ten Donkelaar, Propriospinal fibers interconnecting the spinal
738 enlargements in some quadrupedal reptiles. *J Comp Neurol* **193**, 871-891 (1980).
739 38. R. F. Samara, S. N. Currie, Crossed commissural pathways in the spinal hindlimb
740 enlargement are not necessary for right left hindlimb alternation during turtle swimming. *J*
741 *Neurophysiol* **98**, 2223-2231 (2007).
742 39. J. D. Comer *et al.*, Sensory and spinal inhibitory dorsal midline crossing is independent of
743 Robo3. *Front Neural Circuits* **9**, 36 (2015).
744 40. E. N. Orlino, Jr., C. M. Wong, P. E. Phelps, L1 and GAD65 are expressed on dorsal
745 commissural axons in embryonic rat spinal cord. *Brain Res Dev Brain Res* **125**, 117-130
746 (2000).
747 41. G. Kardon, Muscle and tendon morphogenesis in the avian hind limb. *Development* **125**,
748 4019-4032 (1998).
749 42. C. Lance-Jones, L. Landmesser, Pathway selection by chick lumbosacral motoneurons
750 during normal development. *Proc R Soc Lond B Biol Sci* **214**, 1-18 (1981).
751 43. D. Satoh, C. Pudenz, S. Arber, Context-Dependent Gait Choice Elicited by EphA4 Mutation
752 in Lbx1 Spinal Interneurons. *Neuron* **89**, 1046-1058 (2016).

753 44. I. B. Hogue *et al.*, Fluorescent Protein Approaches in Alpha Herpesvirus Research. *Viruses*
754 **7**, 5933-5961 (2015).
755 45. Y. Hadas *et al.*, A 'tool box' for deciphering neuronal circuits in the developing chick spinal
756 cord. *Nucleic Acids Res* **42**, e148 (2014).
757 46. D. H. Rowitch *et al.*, Identification of an evolutionarily conserved 110 base-pair cis-acting
758 regulatory sequence that governs Wnt-1 expression in the murine neural plate. *Development*
759 **125**, 2735-2746 (1998).
760 47. L. S. Andersson *et al.*, Mutations in DMRT3 affect locomotion in horses and spinal circuit
761 function in mice. *Nature* **488**, 642-646 (2012).
762 48. V. B. Indjeian *et al.*, Evolving New Skeletal Traits by cis-Regulatory Changes in Bone
763 Morphogenetic Proteins. *Cell* **164**, 45-56 (2016).
764 49. E. Z. Kvon *et al.*, Progressive Loss of Function in a Limb Enhancer during Snake Evolution.
765 *Cell* **167**, 633-642 e611 (2016).
766 50. J. P. Himanen *et al.*, Crystal structure of an Eph receptor-ephrin complex. *Nature* **414**, 933-
767 938 (2001).
768 51. O. Pernet, Y. E. Wang, B. Lee, Henipavirus receptor usage and tropism. *Curr Top Microbiol*
769 *Immunol* **359**, 59-78 (2012).
770 52. O. A. Negrete *et al.*, Two key residues in ephrinB3 are critical for its use as an alternative
771 receptor for Nipah virus. *PLoS Pathog* **2**, e7 (2006).
772 53. C. E. Restrepo *et al.*, Change in the balance of excitatory and inhibitory midline fiber
773 crossing as an explanation for the hopping phenotype in EphA4 knockout mice. *Eur J*
774 *Neurosci* **34**, 1102-1112 (2011).
775 54. R. L. Watterson, Development of the glycogen body of the chick spinal cord; normal
776 morphogenesis, vasculogenesis and anatomical relationships. *J Morphol* **85**, 337-389
777 (1949).
778 55. R. L. Watterson, B. E. Spiroff, Development of the glycogen body of the chick spinal cord;
779 effects of unilateral and bilateral leg-bud extirpation. *Physiol Zool* **22**, 318-337, pl (1949).
780 56. J. Korlach *et al.*, De novo PacBio long-read and phased avian genome assemblies correct
781 and add to reference genes generated with intermediate and short reads. *Gigascience* **6**, 1-16
782 (2017).
783 57. A. Filosa *et al.*, Neuron-glia communication via EphA4/ephrin-A3 modulates LTP through
784 glial glutamate transport. *Nature neuroscience* **12**, 1285-1292 (2009).
785 58. Y. Lallemand, V. Luria, R. Haffner-Krausz, P. Lonai, Maternally expressed PGK-Cre
786 transgene as a tool for early and uniform activation of the Cre site-specific recombinase.
787 *Transgenic Research* **7**, 105-112 (1998).
788 59. M. G. Grabherr *et al.*, Full-length transcriptome assembly from RNA-Seq data without a
789 reference genome. *Nat Biotechnol* **29**, 644-652 (2011).
790 60. A. Kania, T. M. Jessell, Topographic motor projections in the limb imposed by LIM
791 homeodomain protein regulation of ephrin-A:EphA interactions. *Neuron* **38**, 581-596
792 (2003).
793 61. W. Halfter, Y. P. Yip, J. W. Yip, Axonin 1 is expressed primarily in subclasses of avian
794 sensory neurons during outgrowth. *Brain Res Dev Brain Res* **78**, 87-101 (1994).
795 62. F. Tie *et al.*, CBP-mediated acetylation of histone H3 lysine 27 antagonizes Drosophila
796 Polycomb silencing. *Development* **136**, 3131-3141 (2009).
797 63. W. A. Whyte *et al.*, Master transcription factors and mediator establish super-enhancers at
798 key cell identity genes. *Cell* **153**, 307-319 (2013).
799

Acknowledgments

The authors thank Tamir Lederman for technical assistance; Jerome Gros for providing the Pacbio p-reads of the quail genome, Wes Warren for providing the Pacbio p-reads of the chicken genome, and Anat Barnea for providing zebra finch hatchlings.

Funding:

This work was supported by a grant to AK and CVM from the US-Israel Binational Science Foundation (grant No. 2017/172), an NSF graduate fellowship to SF, and grants to AK from the Israel Science Foundation (grant No. 1400/16) and the Avraham and Ida Baruch endowment fund.

Author contributions:

AK, CVM, BH: research design, data analysis; BH: circuit analysis, in situ hybridization; OM: circuit analysis; RSM: enhancer analysis; JE: protein studies; SF, PVL: genomics and gene structure analysis; SP, RK: generated conditional ephrin-B3 knockout mouse; AK, CVM: wrote manuscript.

Competing interests:

The authors declare no competing of interest

Data and materials availability:

The data was deposited at any archive.

822 **Figures and Tables**

823 **Figures legends**

824 **Figure 1: Spinal gait circuitry and EFNB3 genomics**

825 **A,B**. A scheme illustrating the morphology and wiring of the spinal cord in wt mouse (A) and in
826 ephrin-B3/EphA4/β2-chimaerin mice collectively referred to as *hop* mutants (B); pre-MN: pre-
827 motoneurons, RP: roof plate. **C.** Simplified cladogram depicting the relations across representative
828 organisms examined in this study. Branch lengths are arbitrary and not calibrated for time, red
829 means EFNB3 is absent in chicken. **D.** Comparison of EFNB3 (red) synteny across organisms where
830 synteny could be examined, with chromosomal location or data source indicated. EFNB3 is absent
831 in Galliformes (red square) and DNAH2 (blue) is absent in birds. Non-avian sauropsids: lizard and
832 alligator; wgs: whole-genome shotgun contigs; HB: hummingbird. **E.** Schematic structure of the
833 predicted mouse and avian ephrin-B3 proteins. RBD: receptor binding domain; TM:
834 transmembrane domain.

835

836 **Figure. 2: Zebra finch ephrin-B3 protein and mRNA expression**

837 **A.** The mouse and zebra finch proteins are presented on the cell membrane. Anti myc antibody
838 (9E10) was used for surface staining of COS-7 cells transiently transfected with amino-terminal
839 myc-tagged ephrin-B3 isoforms. The sequence of the full length zebra finch ephrin-B3 transcript
840 was reconstructed from RNA-seq reads using the Trinity platform (*59*) (Supp. Fig. S1). **B.** Binding
841 assay shows EphA4-AP binding to mouse ephrin-B3 protein but not to GFP or to zebra finch
842 ephrin-B3. **C.** Representative EphA4-AP/ephrin-B3 binding curves assessed by AP activity in a
843 colometric assay. Apparent KD value for mouse ephrin-B3 was 40.15 nM (n=3).**D.** *In situ*
844 hybridization for ephrin-B3 mRNA in P0 zebra finch spinal cord. High expression is evident in the
845 floor plate (FP), but declines along the roof plate (RP). **D'.** Normalized optical density (OD) profile

846 of zebra finch ephrin-B3 midline expression; shown is the means from 58 cross sections. **E.** *In situ*
847 hybridization for ephrin-B3 mRNA in E15.5 mouse spinal cord. High expression is evident in both
848 the FP and RP. **E'.** Normalized optical density (OD) profile of mouse ephrin-B3 midline expression;
849 shown is the means from 160 cross sections. **F,G.** Analysis of the activity of the ephrin-B3
850 enhancer element, at E9 (F) and E15 (G). The cherry reporter gene was cloned downstream to the
851 putative enhancer and electroporated into the chick spinal cord. GFP, under the control of the
852 ubiquitous CAGG enhancer-promoter, was co-electroporated. The reporter is detected in both FP
853 and RP (F,G), similar to the pattern of ephrin-B3 expression in mice, while GFP is expressed
854 ubiquitously.
855
856 **Figure 3: Expression of ephrin-B1, ephrin-B2 and EphA4 mRNAs in the chick spinal cord.**
857 *In situ* hybridization for ephrin-B1 (A,B), ephrin-B2 (C,D) and EphA4 (E,F) mRNAs at the brachial
858 level in E10 (A,C,E) and E16 (B,D,F) cords. The floor plate (FP) is indicated by black arrows and the
859 roof plate (RP) by magenta arrows. **A,B**. Ephrin-B1 at E10 is high in the FP and low in the RP at E16
860 it is high in the FP and low in ventral RP. **C,D.** Ephrin-B2 at E10 is low in the FP and RP; at E16 it is
861 low in ventral RP. **E,F.** EphA4 expression at E10 is widespread in the gray matter, with higher levels
862 in scattered interneurons the lateral subdivision of the lateral motor columns (LMC_l) and the
863 medial motor columns (MMC). At E16, expression is detected in scattered interneurons and
864 motoneurons. Interneurons invading the dorsal midline are apparent (white arrow in inset in F).
865 Insets in E and F are enlargements of the areas boxed in dashed yellow. **E',F'.** Cell density
866 distribution, extracted from 10 cross sections from the regions flanking the dorsal midline at E10
867 and E16, respectively (indicated by white dashed boxes in E and F). **G.** Summation of cell *in situ*
868 hybridization relative intensity in the area indicated in E' (E10, blue) and F' (E16, red). The area
869 along the X was subdivided to 100 epochs. N=10 sections for each experiment. Values are

870 significantly different around the dorsal midline (spanning from -15 to 15) $p<0.0001$, t-test, see
871 Materials and methods and supplementary statistics).
872
873 **Figure 4: Spinal cord morphology in *hop* mutants and chick show enlarged brachial RPs.**
874 **A-D**, Dark field microphotographs of transverse sections of adult mouse spinal cord at lumbar and
875 brachial levels. Compared are control heterozygous (EphA4$^{lx/lx-}$; A,C) and homozygous null mice
876 (EphA4$^{lx/lx-}$/PGK-Cre^{+}; B,D) (*32*). Right insets (enlargements of the boxed areas) depict the central
877 canal and the RP and FP.
878 **E,F.** Transverse sections at the brachial (E) and lumbar (F) levels of E15 chick spinal cord. The white
879 matter is labelled with the anti-neurofilament antibody 3A10, the gray matter with nuclear DAPI
880 staining. Right inset (in E) is an enlargement of the boxed area.
881 **G.** Box plot representation of the roof plate (RP) to floor plate (FP) length ratios at the brachial
882 level in adult EphA4+/- mouse (N= 3, 36 cross sections), adult EphA4-/- mouse (N= 3, 36 sections),
883 E15 chick (N= 2, 22 sections) and P0 zebra finch (N= 1, 25 sections). The difference between the
884 heterozygous mouse, chick and zebra finch groups and the control homozygous null mouse group
885 is statistically significantly (See supplementary statistics). RP: roof plate; FP: floor plate.
886
887 **Figure 5: Midline crossing at the brachial and lumbar levels of chick spinal cord**
888 **A.** Dorsal midline crossing at brachial level in E15 chick demonstrated by neurofilament (3A10)
889 immunostaining in transverse sections. Detail views of three examples in insets, left inset is an
890 enlargement of the boxed area in A. Axons cross at the FP (yellow arrows) and the dorsal part of
891 the RP (white arrows). **B.** Dorsal midline crossing at brachial level in E17 chick; the boxed area is
892 enlarged in B' and B''. Anti-3A10 labels all axons, and anti-TAG1 labels sensory axons (*61*). **C.**
893 Dorsal midline crossing is evident following unilateral expression of a reporter gene. GFP under

894 the control of the CAGG enhancer/promoter construct was electroporated at E3 into the left side
895 of the spinal cord. At E15, midline-crossing axons are evident in the brachial FP (yellow arrows)
896 and RP (white arrows) . Detail views of three examples in insets, left inset is an enlargement of the
897 boxed area in C. **D,E.** Transverse sections at the sciatic plexus level at E15 (D) and E17 (E). Axons
898 cross only at the FP (yellow arrows). The glycogen body (GB) lacks axonal labelling. **F.** Transverse
899 section at the crural plexus level at E17. Right inset is an enlargement of the boxed area in F.
900 Axons cross at the FP (yellow arrow) and RP (white arrow). **G.** Box plot of the ratio between axons
901 crossing the RP and the FP at different axial levels in E15 chick. Numbers of midline-crossing axons
902 were scored at cervical (15 sections), brachial (31 sections), thoraxic (27 sections), lumbar crural
903 (23 sections) and lumbar sciatic (14 sections) levels of one embryo. At the sciatic level axons did
904 not cross the glycogen body. (See supplementary statistics). RP: roof plate; FP: floor plate.
905

906 **Figure 6: Patterns of pre-MNs in the brachial and lumbar chick spinal cord**

907 **A-C.** Cell distribution maps in the brachial and lumbar segments of E15 spinal cord sections of
908 chicks in which the hindlimb (A), distal wing (B), or pectoral (C) musculature were injected with
909 PRV-cherry at E14. Data are from 1038 ipre-MNs and 88 cpre-MNs in A (3 embryos), 620 ipre-MNs
910 and 210 cpre-MNs in B (4 embryos) and 734 ipre-MNs and 392 cpre-MNs in C (2 embryos). Ellipses
911 in dashed magenta represent the areas occupied by motoneurons. A'-C'. Images of PRV-positive
912 neurons supplemented with immunostaining for motoneurons (ChAT); right insets are
913 enlargements of the midline boxed area showing axonal decussation of pre-MNs at the FP (yellow
914 arrows) and RP (white arrows); white ellipses represent the central canal.

915 **D.** Identification of a subpopulation of pre-MNs that innervate pectoral muscle motoneurons
916 bilaterally. PRV-GFP and PRV-cherry were injected bilaterally at E14 into the pectoral muscles. Cell
917 distribution map of bilaterally innervating pectoral pre-MNs seen at E15 is shown in gray. D'.

918 Examples of bilaterally innervating pre-MNs; left panels: merged images; middle panels: PRV-
919 cherry; right panels: PRV-GFP. Out of 500 and 730 cpre-MNs on each side (18 sections), 11.9% ±
920 0.05 and 10.9% ± 0.04 were double labeled.
921
922 **Figure 7: Expression of exogenous ephrin-B3 in the chick RP prevents midline crossing**
923 **A.** Strategy for ectopic expression of the mouse ephrin-B3 at the roof plate. **B.** Cross-section from
924 brachial spinal cord of E17 embryo expressing ephrin-B3 (magenta) at the dorsal midline,
925 immunostained for neurofilament (cyan). **C,D.** Magnifications of 3 examples of dorsal midline
926 region of spinal cords electroporated with GFP (C,C',C") or ephrin-B3 (D,D',D") (both in magenta),
927 immunostained for neurofilament (cyan). The black and white images are the neurofilament
928 (3A10) staining. Some neurites cross the GFP-expressing RP (C) but not the ephrin-B3-expressing
929 RP. **E.** Quantification of dorsal midline crossing in spinal cords expressing GFP (N=43 sections, 3
930 embryos), mouse ephrin-B3 (N=71 sections, 3 embryos) or ephrin-B3-ΔC (N=59 sections, 3
931 embryos). The numbers of neurites crossing ephrin-B3- or ephrin-B3-ΔC-expressing RPs were
932 significantly lower than in GFP-expressing controls (See supplementary statistics).
933
934 **Figure 8: Expression of exogenous ephrin-B3 in the chick RP prevents pre-MN crossing**
935 **A.** Schematic of the experimental setup. GFP or ephrin-B3 were expressed in the midline at E3. At
936 E14, PRV-cherry was unilaterally injected into the wing musculature, and embryos fixed and
937 processed 38 hr later. ChAT-immunostained (cyan) motoneurons (MN)and PRV-labeled (magenta)
938 pre-MNs are indicated; dashed line represents cpre-MN axons that cross the RP. **B,C.** Transverse
939 sections of control (B) and Wnt1::ephrin-B3-expressing E15 embryos (3 examples in C,C'C"). The
940 black and white images are in B' and the insets in C,C',C" are PRV staining. In the control (B), cpre-
941 MNs somata are located ventral and dorsal to the central canal and neurites of cpre-MNs are

942 apparent at the FP (yellow arrows in B') and RP (white arrows in B'). In Wnt1::mEFNB3 embryos
943 (C, C', C''), the somata of pre-MNs are mainly located ventral to the central canal. Axons crossing
944 the FP (yellow arrows) and few short neurites (white arrowheads) crossing the dorsal midline are
945 shown in the right insets. **D.** Density maps of brachial cpre-MNs in control (GFP, N = 880 cells from
946 six embryos) and five ephrin-B3-expressing embryos (N = 242, 467, 366, 49 and 67 cells). The
947 fraction of sections containing ephrin-B3 expression along the entire dorsal midline is indicated at
948 the upper part of each spinal cord. A ventral shift of the distribution is apparent in the high
949 efficiency electroporated spinal cords of wnt1-B3-4 and wnt-1-B3-5. **E-H.** Plots demonstrating the
950 correlation between ventral commissural/ipsilateral, commissural/Ipsilateral, dorsal
951 commissural/ipsilateral and dorsal commissural/ ventral commissural pre-MNs ratios to the
952 electroporation efficiency (as described in D), respectively. **I,J.** Schematic illustration of the
953 circuitry at the lumbar (I) and brachial (J) avian spinal cord. We propose that dorsal midline
954 crossing is prevented at the lumbar level by the glycogen body, while dorsal midline crossing at
955 the brachial level is enabled due to the loss of ephrin-B3 activity. The brachial avian spinal cord
956 shares significant morphological and wiring similarities with mouse *hop* mutants.

Fig. 1

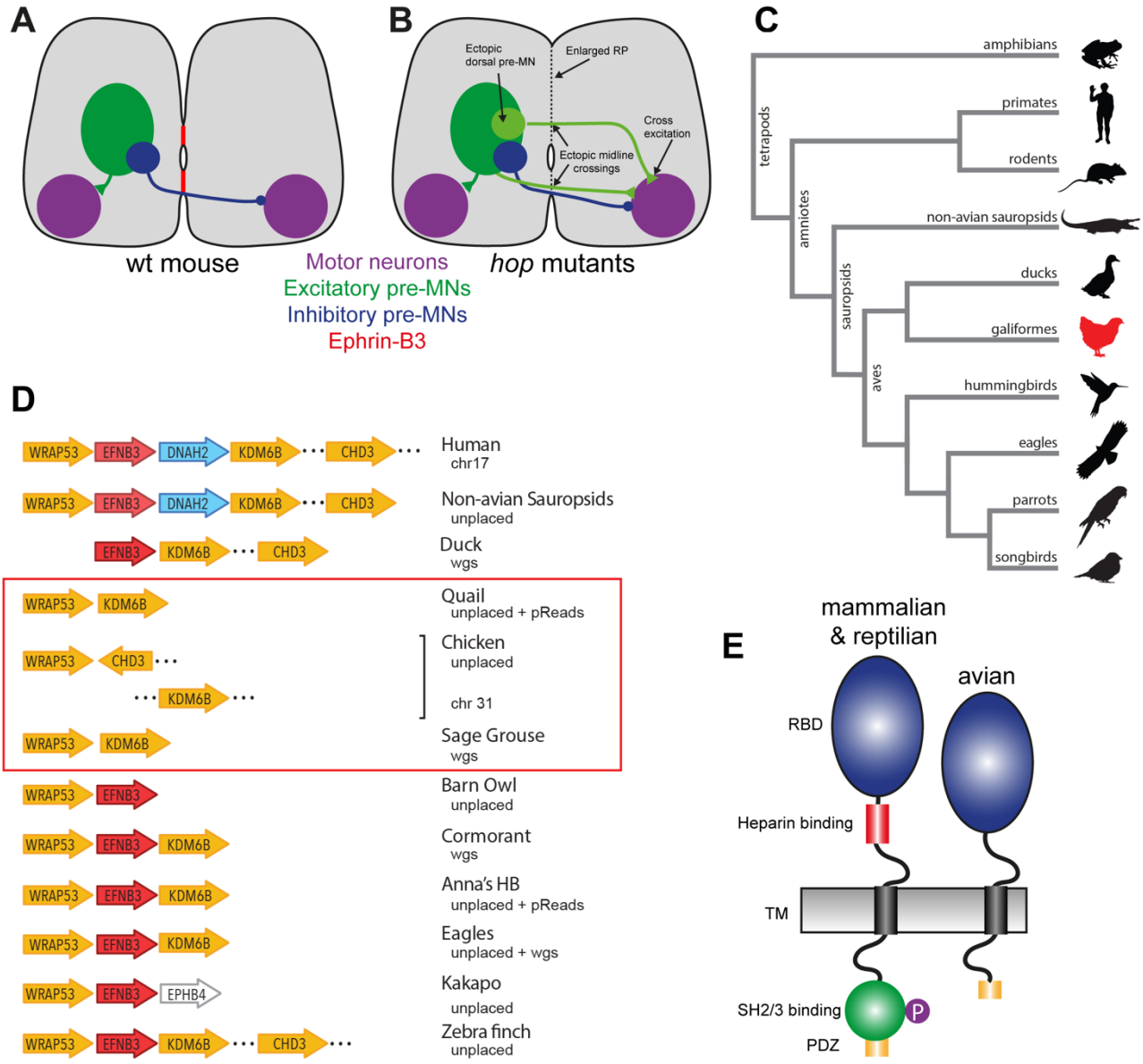
A
B
C
D
E
wt mouse
hop mutants
Ectopic dorsal pre-MN
Enlarged RP
Cross excitation
Ectopic midline crossings
Motor neurons
Excitatory pre-MNs
Inhibitory pre-MNs
Ephrin-B3
amphibians
primates
rodents
non-avian sauropsids
ducks
galiformes
hummingbirds
eagles
parrots
songbirds
tetrapods
amniotes
sauropsids
aves
WRAP53
EFNB3
DNAH2
KDM6B
CHD3
EPHB4
Human
chr17
Non-avian Sauropsids
unplaced
Duck
wgs
Quail
unplaced + pReads
Chicken
unplaced
chr 31
Sage Grouse
wgs
Barn Owl
unplaced
Cormorant
wgs
Anna's HB
unplaced + pReads
Eagles
unplaced + wgs
Kakapo
unplaced
Zebra finch
unplaced
mammalian & reptilian
avian
RBD
Heparin binding
TM
SH2/3 binding
PDZ
P

957

Figure 2

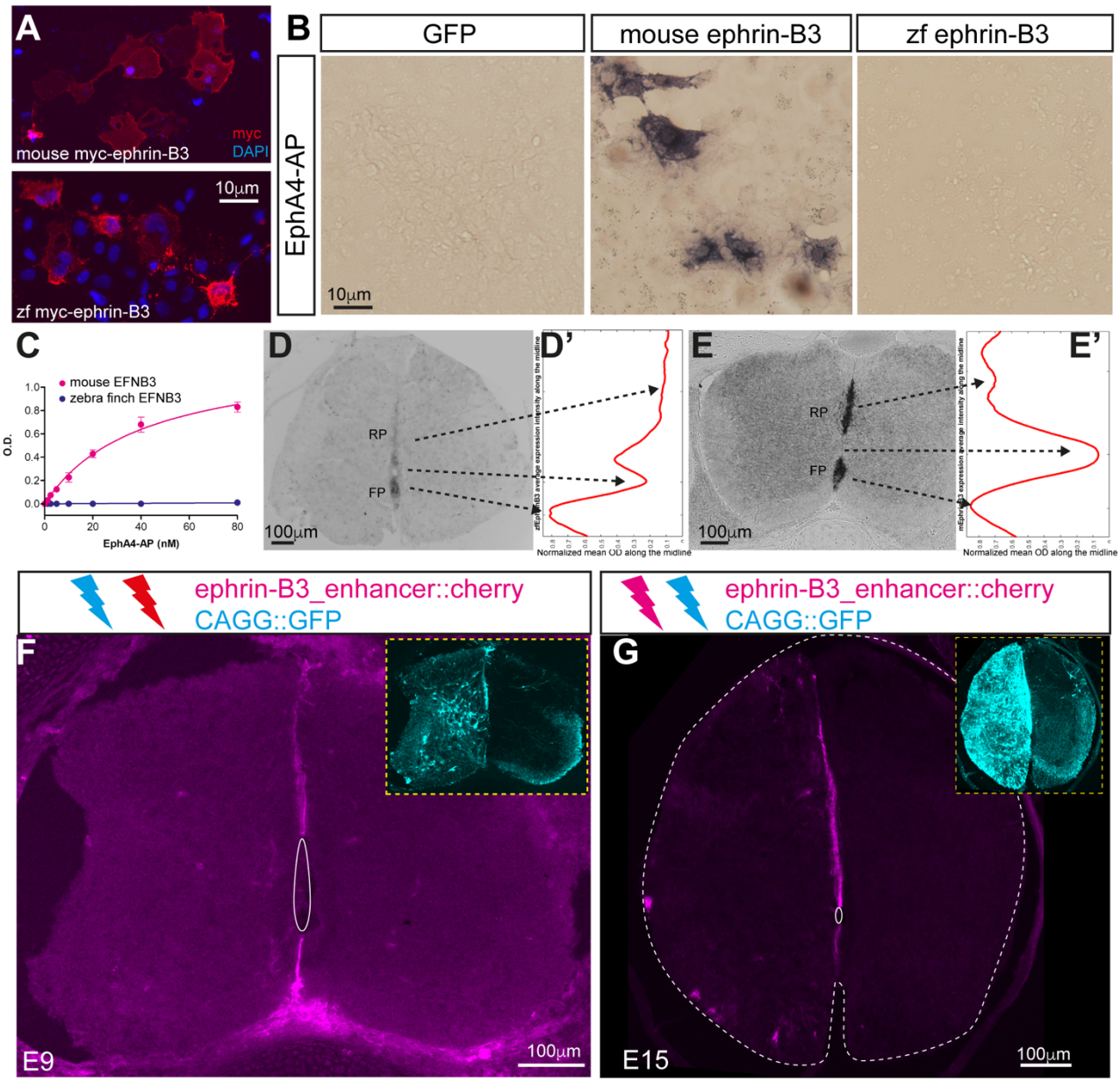
A
mouse myc-ephrin-B3
myc
DAPI
10μm
zf myc-ephrin-B3
B
GFP
mouse ephrin-B3
zf ephrin-B3
EphA4-AP
10μm
C
mouse EFNB3
zebra finch EFNB3
O.D.
EphA4-AP (nM)
D
RP
FP
100μm
D'
Normalized mean OD along the midline
E
RP
FP
100μm
E'
Normalized mean OD along the midline
ephrin-B3_enhancer::cherry
CAGG::GFP
F
E9
100μm
ephrin-B3_enhancer::cherry
CAGG::GFP
G
E15
100μm

958

Fig. 3

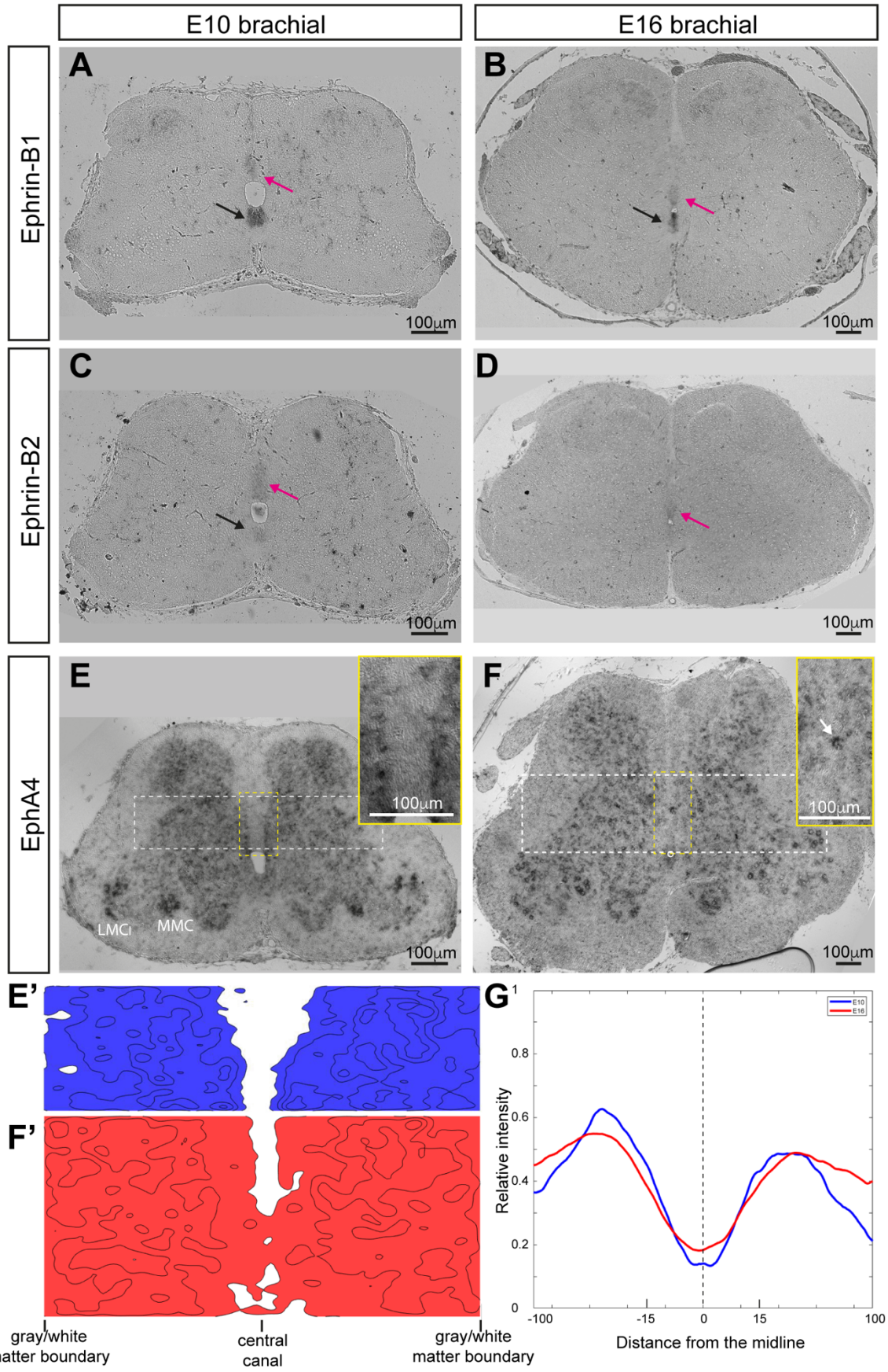
E10 brachial
E16 brachial
Ephrin-B1
Ephrin-B2
EphA4
A
B
C
D
E
F
100μm
LMCl
MMC
E'
F'
G
E10
E16
Relative intensity
Distance from the midline
gray/white matter boundary
central canal
gray/white matter boundary

959

Fig. 4

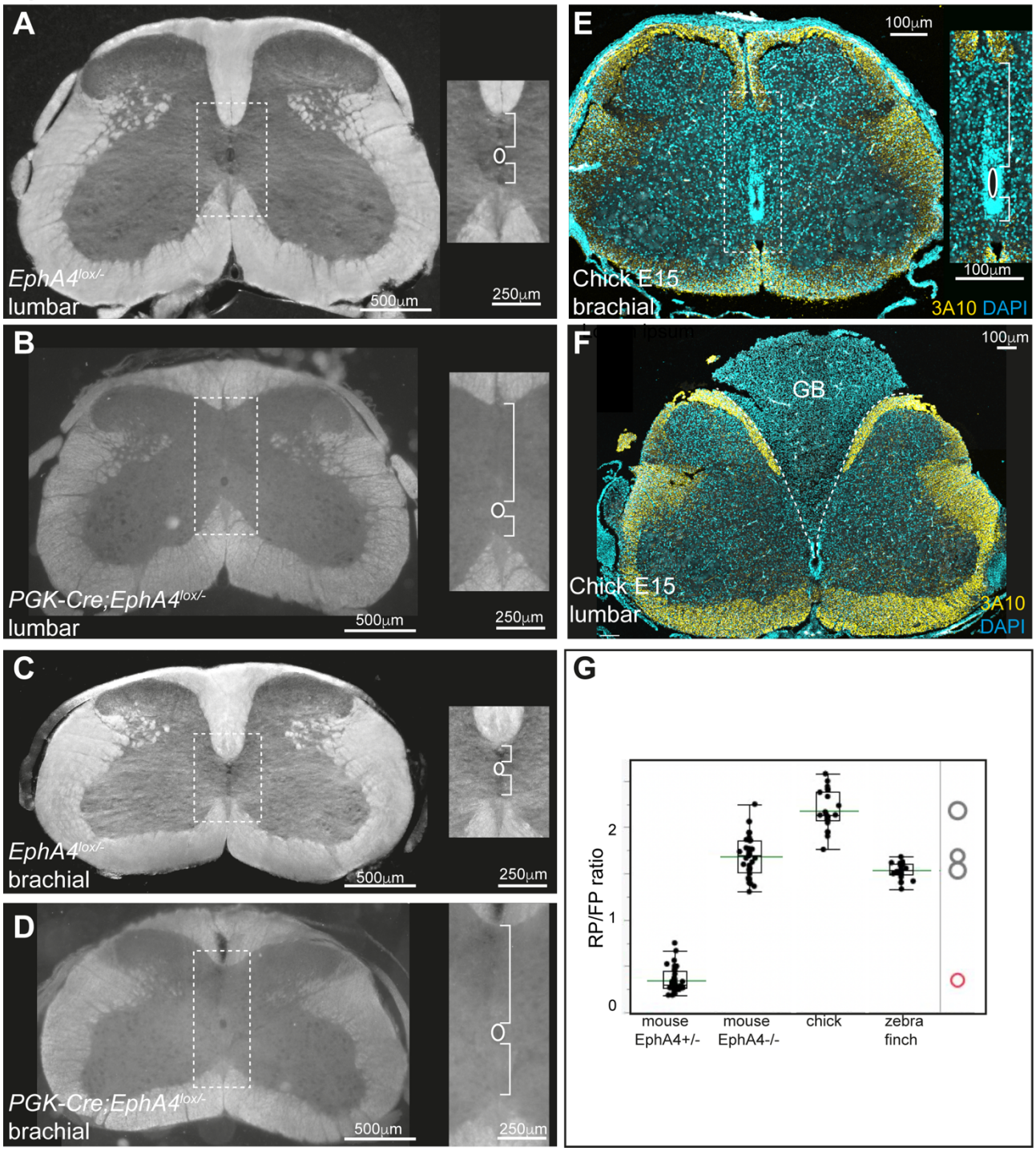
A
EphA4lox/-
lumbar
500µm
250µm
B
PGK-Cre;EphA4lox/-
lumbar
500µm
250µm
C
EphA4lox/-
brachial
500µm
250µm
D
PGK-Cre;EphA4lox/-
brachial
500µm
250µm
E
100µm
Chick E15
brachial
100µm
3A10 DAPI
F
100µm
GB
Chick E15
lumbar
3A10
DAPI
G
RP/FP ratio
0
1
2
mouse
EphA4+/-
mouse
EphA4-/-
chick
zebra
finch

960

Fig. 5

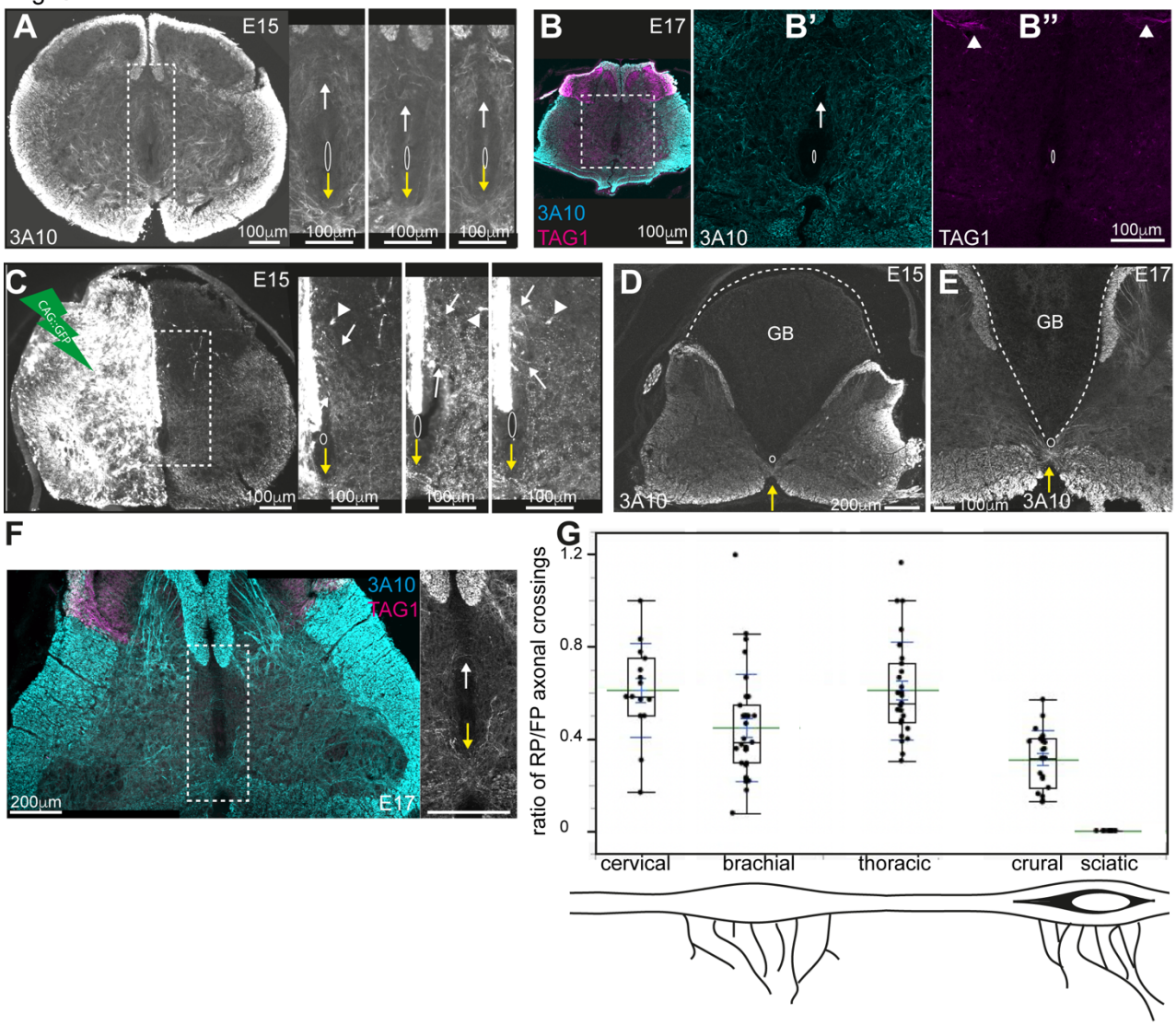
A
E15
3A10
100μm
B
E17
3A10
TAG1
B'
B''
TAG1
C
CAG-GFP
D
GB
200μm
E
F
200μm
G
ratio of RP/FP axonal crossings
1.2
0.8
0.4
0
cervical
brachial
thoracic
crural
sciatic

961

Fig. 6

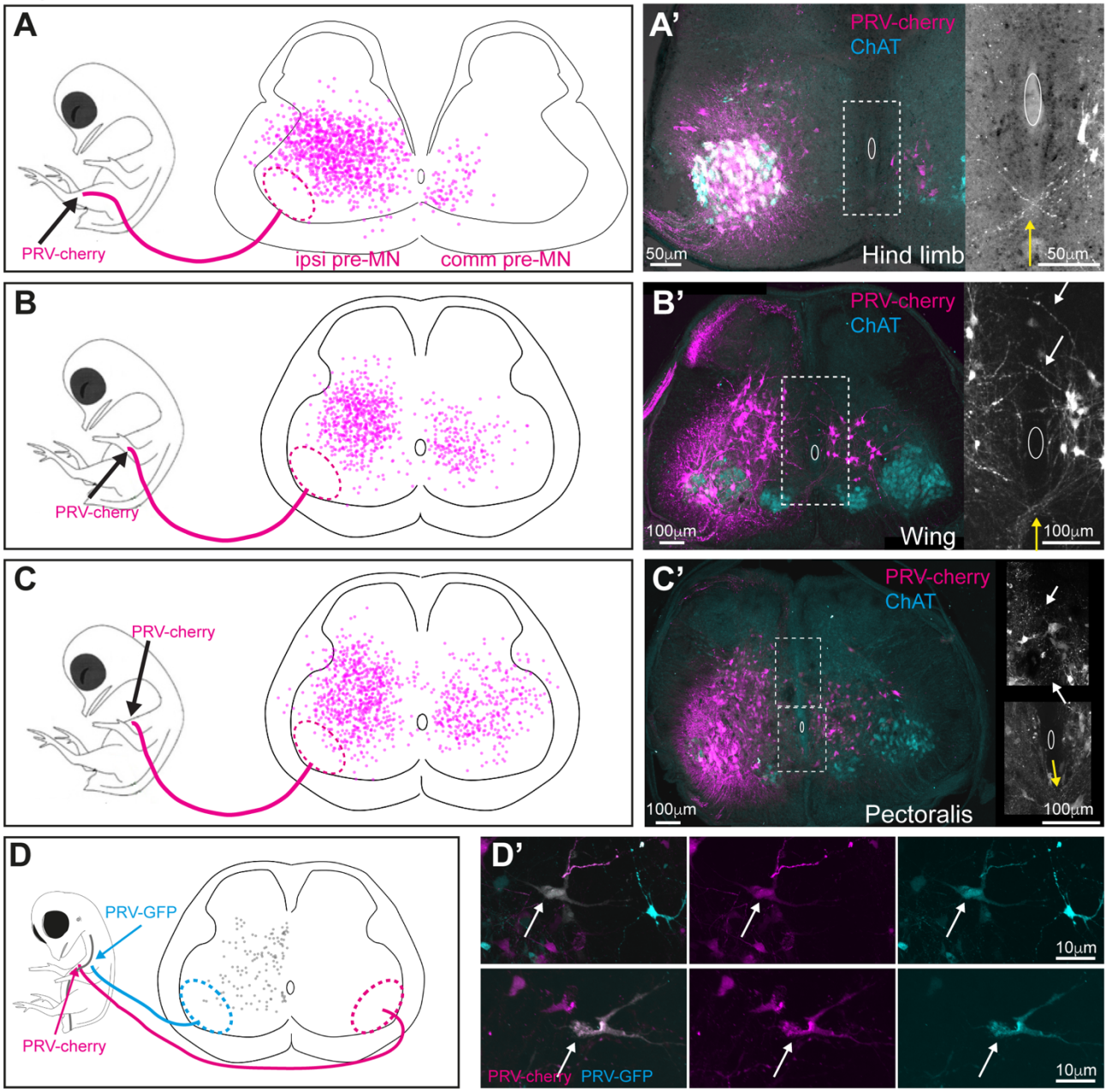
A
PRV-cherry
ipsi pre-MN
comm pre-MN
A'
PRV-cherry
ChAT
50μm
Hind limb
50μm
B
PRV-cherry
B'
PRV-cherry
ChAT
100μm
Wing
100μm
C
PRV-cherry
C'
PRV-cherry
ChAT
100μm
Pectoralis
100μm
D
PRV-GFP
PRV-cherry
D'
10μm
PRV-cherry PRV-GFP
10μm

962

Fig. 7

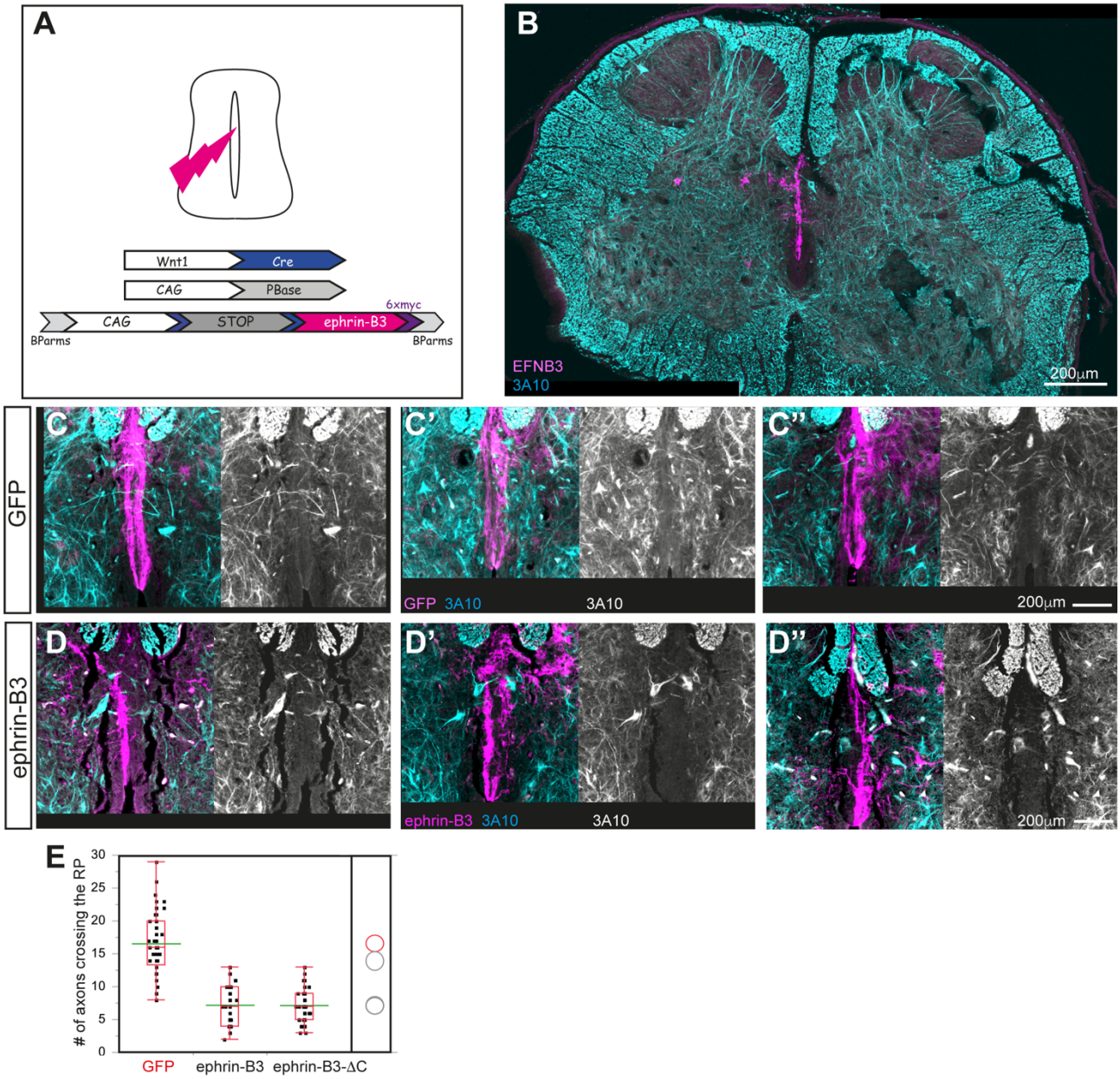
A
Wnt1
Cre
CAG
PBase
6xmyc
CAG
STOP
ephrin-B3
BParms
BParms
B
EFNB3
3A10
200μm
GFP
C
C'
C''
GFP 3A10
3A10
200μm
ephrin-B3
D
D'
D''
ephrin-B3 3A10
3A10
200μm
E
# of axons crossing the RP
0
5
10
15
20
25
30
GFP
ephrin-B3
ephrin-B3-ΔC

963

Fig. 8

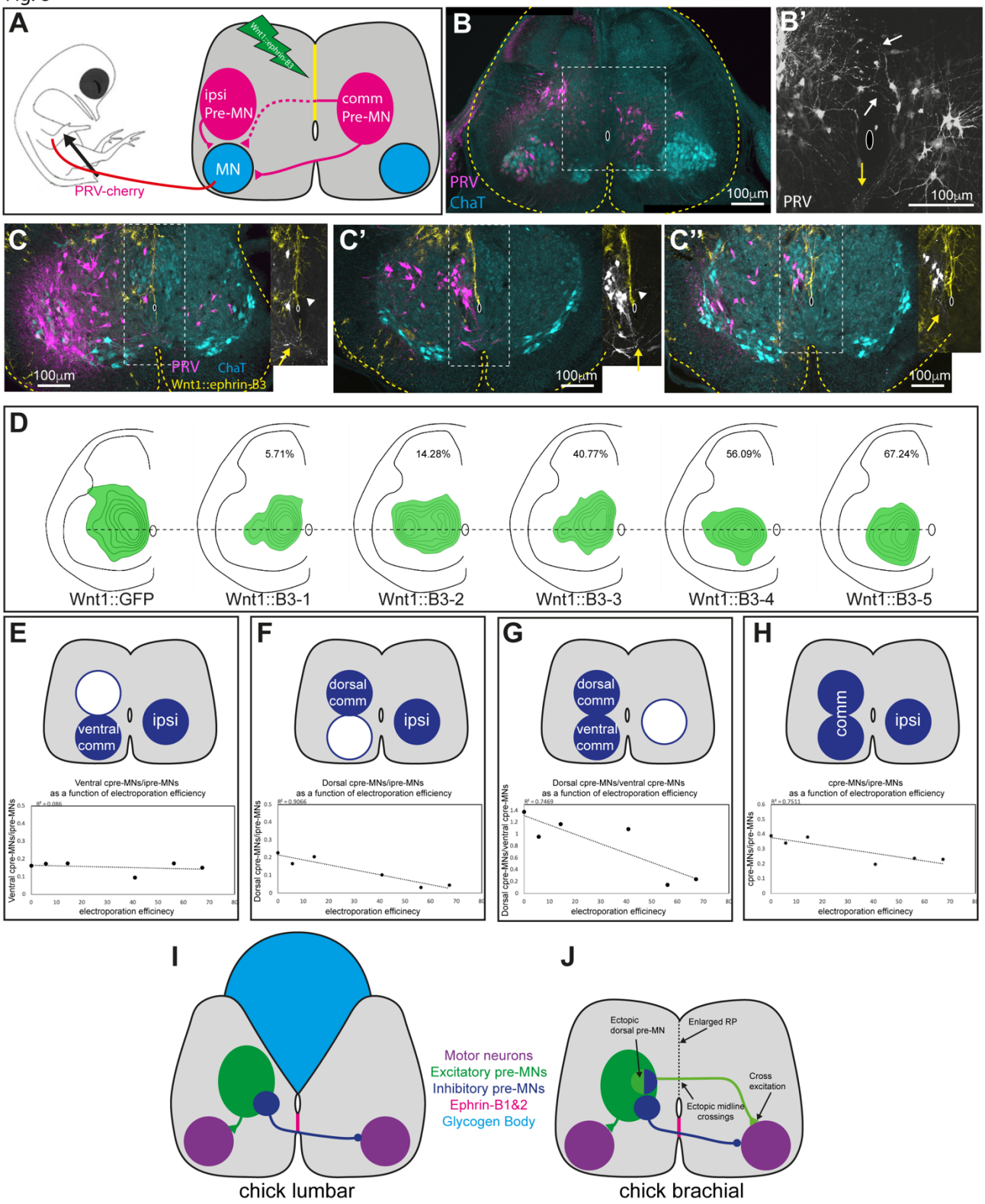
A
Wnt1::ephrin-B3
ipsi
Pre-MN
comm
Pre-MN
MN
PRV-cherry
B
PRV
ChaT
100μm
B'
PRV
100μm
C
100μm
PRV
ChaT
Wnt1::ephrin-B3
C'
100μm
C''
100μm
D
5.71%
14.28%
40.77%
56.09%
67.24%
Wnt1::GFP
Wnt1::B3-1
Wnt1::B3-2
Wnt1::B3-3
Wnt1::B3-4
Wnt1::B3-5
E
ventral comm
ipsi
Ventral cpre-MNs/ipre-MNs as a function of electroporation efficiency
Ventral cpre-MNs/ipre-MNs
electroporation efficiency
F
dorsal comm
ipsi
Dorsal cpre-MNs/ipre-MNs as a function of electroporation efficiency
Dorsal cpre-MNs/ipre-MNs
electroporation efficiency
G
dorsal comm
ventral comm
Dorsal cpre-MNs/ventral cpre-MNs as a function of electroporation efficiency
Dorsal cpre-MNs/ventral cpre-MNs
electroporation efficiency
H
comm
ipsi
cpre-MNs/ipre-MNs as a function of electroporation efficiency
cpre-MNs/ipre-MNs
electroporation efficiency
I
chick lumbar
Motor neurons
Excitatory pre-MNs
Inhibitory pre-MNs
Ephrin-B1&2
Glycogen Body
J
Ectopic dorsal pre-MN
Enlarged RP
Cross excitation
Ectopic midline crossings
chick brachial

964
965

Supplementary Materials for

Natural loss of function of ephrin-B3 shapes spinal flight circuitry in birds

Baruch Haimson[1], Oren Meir[1], Reut Sudakevitz-Merzbach[1], Gerard Elberg[1], Samantha Friedrich[3], Peter V. Lovell[3], Sónia Paixão[2], Rüdiger Klein[2], Claudio V. Mello[3*] and Avihu Klar[1*]

* Avihu Klar. Email: avihu@mail.huji.ac.il
* Claudio V. Mello. Email: melloc@ohsu.edu

This PDF file includes:

Supplementary Text
Figs. S1 to S6
Tables S1
References (59,62,63)

Fig. S1. Ephrin-B3 gene and transcripts in zebra finch

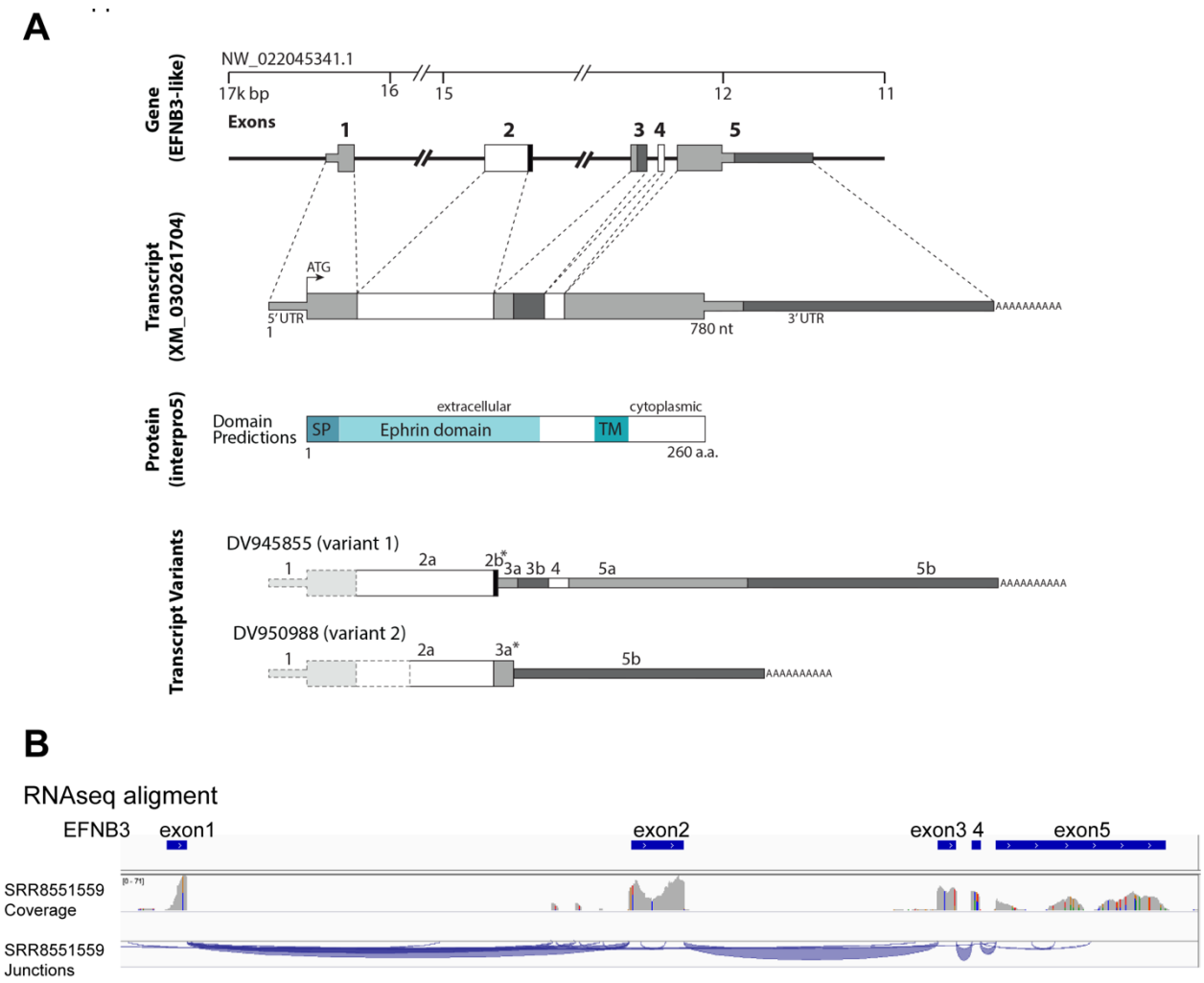

C

```
GGCGGCGGCGGCGGCGGCGGCGGCGGCGGCGGAGCGGGGGGCGGCCGGGGCCCACCGGGAGGGGCCCAGAGCGGC
CGGGGGGCGCCGGGGCCCGGCGGGGCGGGGGGCGATGGCGGGGCGGGCGGCGGCGCTGCTGGTGGCCGTGCTGGG
CGCGGGGGCCGCGGGGCTGAGCCTGGAGCCGGTGGTCTGGCACACGGGGAACCGGCGGTTCCTGGAGGCCGGCGG
TTACGTGCTGTACCCGCAGATCGGTGACCGCCTGGACCTGGTGTGCCCGGGGGGCGCGGGGTACGAGTACTACAA
GCTGTACCTGGTGGGGGGGGCGCAGGCGCGGCGCTGCCAGGTGCCCCCCGCGCCCACCCTGCTGCTGACCTGCGA
CCGCCCCCAGCGCGACGTGCGCTTCACCATCAAGTTCCAGGAGTTCAGCCCCAACCTCTGGGGCCACGAGTTCCG
CCGCCAGCACGACTATTACATCATCACCACCTCGGACGGGACCCCCGAGGGGCTGGAGAACCGCCAGGGCGGGGC
CTGCCTGACCCGGGCCATGCGGGTCACCCTGCGCGTGGGGCAGCGCCCCGGGGCGGAGACACCGCCGGAGCAGGA
TGGGACAGGTTCAGCCAATCAGACGAGCCCGCCCGGGCCGGGCCCGCCCCCCGCGCGGGGAGGGGCGGAGCTGTG
GGGCGCGGGGGGAGGGGCGGCGCTGCTGGCGCTGGGGGGGGCGGGGGGGGCGCTCTGGTGGCGGCGCCGCCCCCG
GAGACCCCCAAAAACTCCACGGGGTGGGGGAGGGGCGGGGCCAACCCGGCCACGCCCCCACGGGCCCGGCCCCGC
CCACCCCCTGCGCGAGCTGCCCCTCCCCCCCGCCGCCCCTCCCCCCACCTACTACAAGGTGTGAGGGGTGGGGGA
GGGGCGGGACACCCAAACTGGGACGGGCCACGCCCACAAAGGGAAGGACACGCCCCACCCTGAAGCTCCGCCCCC
TCGGGGCAAAGGGGAATGACGGACCCAAAAAGGGAAGAATTTGCCCCAAATTGACCCCCCAGGTCTGGATGGGTG
TGGCTTAACCGGGAGGCGTGGCCTGAATTGGGCGTGGTCACTAAAGGGGTGTGGCTGTGATGTCATATGGTGCCG
CCCAGTGGGCGTGGTCAAATATGGGCGTGGTCTCCATAAATGGGCGTGGCTTTACCTGGGGAGGCGGAGCTTAAA
TGGCTTTGAGGCGTCACCCCTGGGAAAGGGGCGGGGCTCGCTCACGGCTCCCTCCCATTGGTCACGATGAAGCCC
CGCCCACACAAAGGGGGCGGAGCTTTCCCGGCGCAGTAACATGGCCGCCGCCACAGCGGATGAACAGGAAGTGAC
GTCACGGCGACAGAGAGGCGGGACTTCCTGTGTGATGTCGCGTGGGGGCGGGGCCTGCGCGCGCGGCTGCTGCTG
ATTAGACAGTTTTGTGCAAAAAAAAAAAAAAAA
```

A. Zebra finch ephrin-B3 gene, predicted transcript, predicted protein, and transcript variants. The two EST clones that include coding exons are DV945855 and DV950988. Both include frameshifts that result in premature *termination (indicated by asterisks)*.

994 B. RNAseq reads of Ephrin-B3 in zebra finch. RNAseq data in zebra finches provide expression
995 support for this structure and for expression of all five exons, and is consistent with the predicted
996 polyA site based on multiple ESTs.
997 C. The sequence of the full length zebra finch ephrin-B3 transcript was reconstructed from RNA-
998 seq reads using the Trinity platform *(59).* The coding exons are indicated in alternating blue and
999 yellow colors. The 5'UTR (black) is included in the 1st exon and the 3'UTR (black) is included in the
1000 5th exon.
1001 .

Fig. S2. Phylogeny of the ephrin-B3 protein

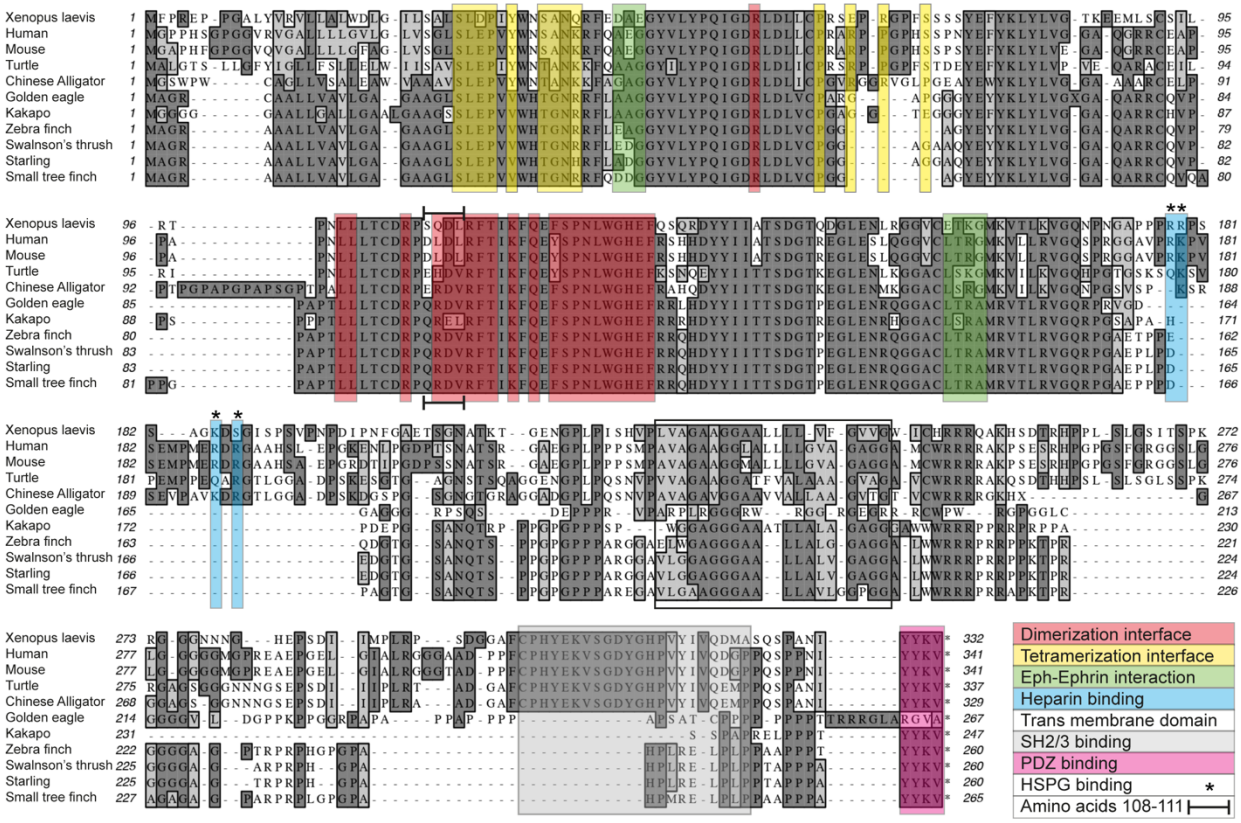

Sequence alignment of the predicted ephrin-B3 proteins from different species. The T-Coffee algorithm was used for alignment of multiple sequences. Avian-specific deletions were detected in the heparin binding, tetramerization interface and SH2/3-binding domains (indicated by blue - with asterisks, yellow and gray rectangles, respectively), and specific mutations observed in the dimerization interface domain (indicated by red rectangles and horizontal bars in residues 108-111 of mouse). The open box indicates the transmembrane domain.

1011 Fig. S3. A putative EFNB3 enhancer in mouse DNAH2

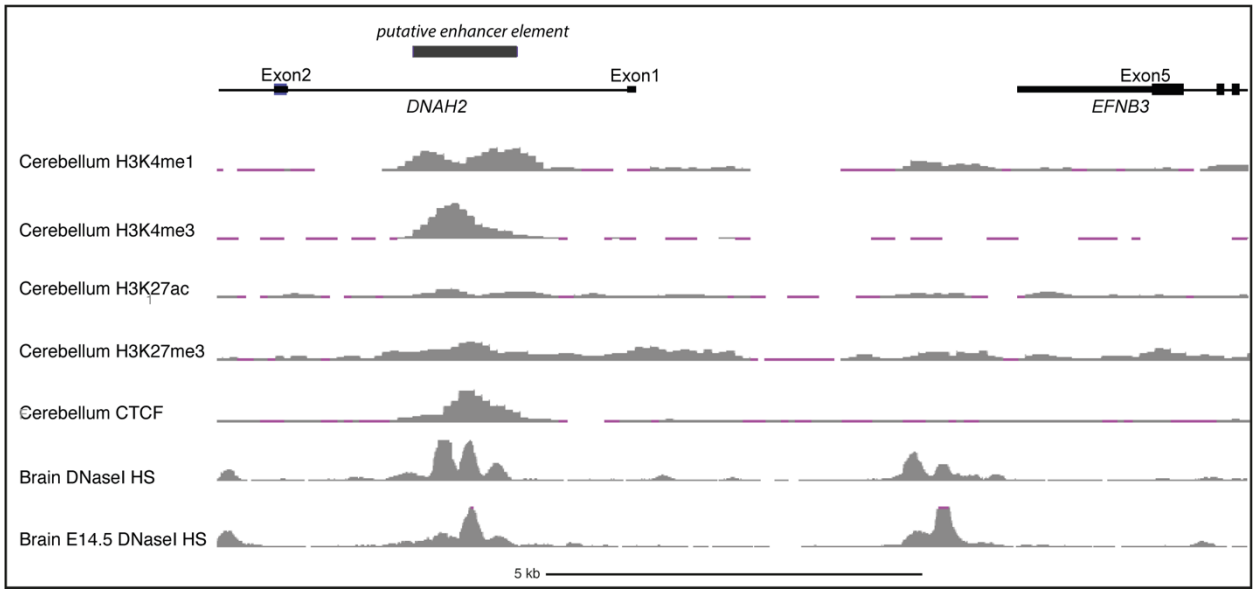

1012
1013

1014 A display of ENCODE analysis of candidate cis-Regulatory elements in mouse chr11:69,546,195-
1015 69,547,544; shown is the region that includes EFNB3 (exons 3-5) and DNAH2 (exons 1-2) genes on
1016 the minus strand. A DNaseI hypersensitive (HS) site is in the 1st intron of DNAH2
1017 (chr11:69,546,195-69,547,544 in GRCm38/mm10). This motif binds modified histones (H3K4me3,
1018 H3K4me1 and H3K27ac) that are associated with active enhancers; histone H3K27me3 is
1019 associated with repression of developmental genes, as well as CTCF – a nuclear factor associated
1020 with active enhancers *(61,62).* Binding of these proteins is apparent in the mouse embryonic
1021 cerebellum and brain. The data was obtained from UCSC genome browser
1022 (https://genome.ucsc.edu/index.html).
1023

1024 Fig. S4. RP/FP ratio along the longitudinal axis of wt mice

1025

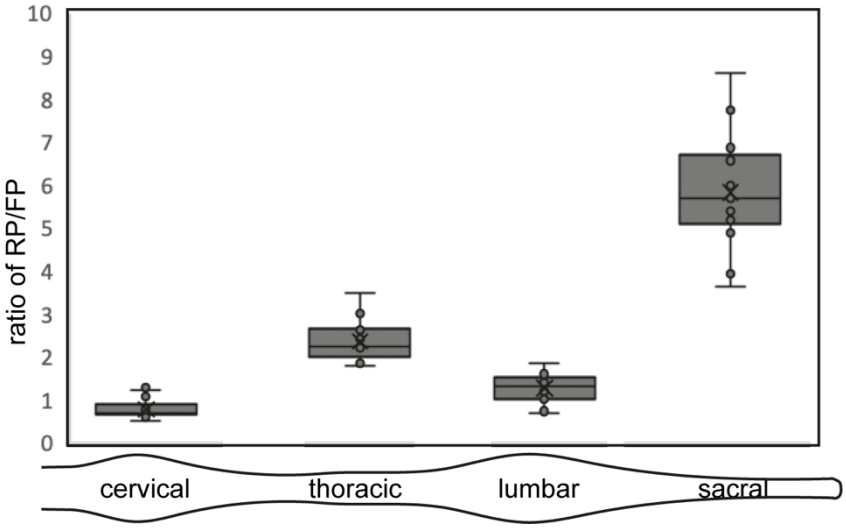

1026

1027

1028 The ratio between the roof plate and floor plate lengths at different segmental levels. The limb-
1029 innervating segments exhibit a lower RP/FP ratio compared to the thoracic and sacral levels.
1030 Analysis was done on images from the Mouse spinal cord atlas (Allen Institute for Brain Science; N
1031 = 17 mice, 15-16 section per mouse). Box plot representation of the roof plate (RP) to floor plate
1032 (FP) length ratios at the cervical, thoracic, lumbar and sacral levels at P4.

1033

1034

1035

1036 **Fig. S5. Distribution of pre-MNs at the spinal crural plexus level**

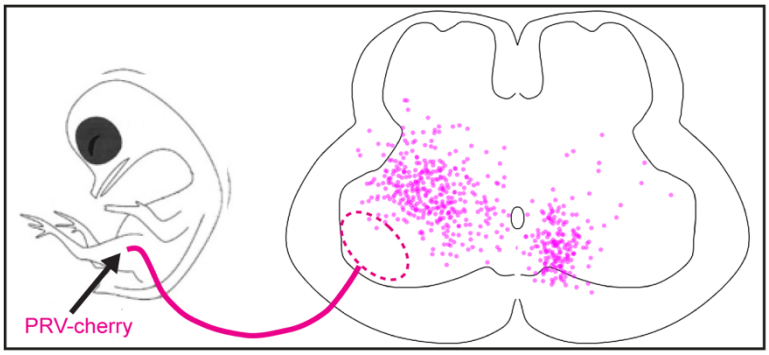

1037
1038
1039 pre-MN map at the crural lumbar level; shown are 361 ipre-MNs and 192 cpre-MNs, respectively (N=3 embryos).
1040

1041 Fig. S6. Brachial pre-MN neurotransmitter identity

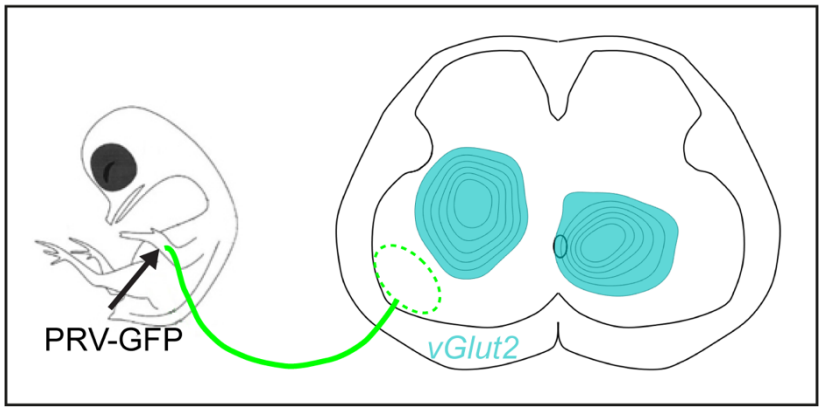

1042

1043 Experimental design for brachial pre-MN labeling and *in situ* hybridization for VGlut2. Density
1044 maps of ipre-MNs and cpre-MNs are shown.

1045
1046

1047 Table S1. The ratio of excitatory pre-MNs in the lumbar and brachial levels of the chick spinal cord.
1048

level	side	% vGlut2	#
Lumbar sciatic	ipsi	46.46	145
	comm	38.62	145
brachial	ipsi	35	274
	Ventral comm	38	29
	Dorsal comm	47	51

1049
1050

1051 **Supplementary References**
1052

1053 59 Grabherr, M. G. *et al.* Full-length transcriptome assembly from RNA-Seq data without a
1054 reference genome. *Nat Biotechnol* **29**, 644-652, doi:10.1038/nbt.1883 (2011).

1055 62 Tie, F. *et al.* CBP-mediated acetylation of histone H3 lysine 27 antagonizes Drosophila
1056 Polycomb silencing. *Development* **136**, 3131-3141, doi:10.1242/dev.037127 (2009).

1057 63 Whyte, W. A. *et al.* Master transcription factors and mediator establish super-enhancers at
1058 key cell identity genes. *Cell* **153**, 307-319, doi:10.1016/j.cell.2013.03.035 (2013).

1059